

國立交通大學

電子物理系

碩士論文

RuO₂和IrO₂的電子傳輸性質



Electronic transport properties in RuO₂ and IrO₂ nanowires

研究生：包智傑

指導教授：陳煜璋 教授

中華民國九十八年七月

RuO₂ 和 IrO₂ 的電子傳輸性質

Electronic transport properties in RuO₂ and IrO₂ nanowires

研究生：包智傑

Student : Jhih-Jie Bao

指導教授：陳煜璋

Advisor : Yu-Chang Chen

國立交通大學

電子物理系



碩士論文

A Thesis

Submitted to Department of Electrophysics

College of Science

National Chiao Tung University

in partial Fulfillment of the Requirements

for the Degree of

Doctor of Philosophy

in

Electrophysics

July 2009

Hsinchu, Taiwan, Republic of China

中華民國九十八年七月

RuO₂ 和 IrO₂ 的電子傳輸性質

學生：包智傑

指導教授：陳煜璋

國立交通大學電子物理學系（研究所）碩士班

摘要

二氧化鈦 (RuO₂) 和二氧化銱 (IrO₂) 在高溫下具有良好的導電性和穩定性。我們用第一原理去研究不同口徑下 RuO₂ 和 IrO₂ 的電子傳輸性質，在計算的方法裡，我們運用密度泛函理論 (Density Functional theory) 去最佳化 RuO₂ 和 IrO₂ 的結構和用局部密度近似法 (Local Density approximation) 去近似。經過計算結果我們可以得到不同口徑下 RuO₂ 和 IrO₂ 奈米線的聲子色散關係而且發現聲速和 Debye 溫度隨著材料的尺寸增加而增加。藉著 Bloch-Gruneisen 方程式可以知道在低溫下，來自於電子聲子交互作用的電阻率隨著溫度五次方成正比而且在同樣溫度下，聲速和 Debye 溫度導致電阻率隨著奈米線的半徑增加而增加。

Electronic transport properties in RuO_2 and IrO_2 nanowires

學生：Jhih-Jie Bao

指導教授：Yu-Chang Chen

Department (Institute) of Electrophysics
National Chiao Tung University

Abstract

RuO_2 and IrO_2 are the inviting electrical contact materials which exhibit the metallic conductivity properties at room temperatures. They crystallize in the rutile structures and display good thermal stability at high temperatures. We study the size effects of the transport properties of RuO_2 and IrO_2 nanowires using first-principles approaches. The relaxed structures of RuO_2 and IrO_2 bulk and nanowires are obtained based on the density functional theory. By using the force tensor we calculate the phonon dispersion relation of the RuO_2 and IrO_2 nanowires with different diameters. We observe that the sound velocities and the Debye temperatures display size effects. According to the Bloch-Gruneisen model within Matthiessen's rule, the resistivity varies as T^5 at low temperatures due to electron-phonon interactions. At the same temperatures, the size effects of the sound velocity and the Debye temperatures lead to the increase of the resistivity as the diameters of the nanowires increase.

致謝

感謝陳煜璋老師這兩年的細心教導，讓我在這期間學會了很多的事情，在寫這篇論文的時候，能夠很有耐心的與我討論以及修改，使得這篇論文更完善。

在這學習的期間，還要感謝研究室裡與學弟們的討論，他們在這之間幫忙了很多的事情，使得我在研究和生活的事務上可以順利的進行。

另外要謝謝和我住在一起的大學同學們，沒有他們陪我玩樂和吃雞塊，我想在這碩士的生活裡會變的很枯樸乏味，以及天天陪我游水的那位同學，可以和我一起分享寫論文的心得，使我在寫論文的時候能夠更面面俱到。

最後要感謝我的父母，默默的支持我和適時的給我鼓勵，再次，謝謝所有幫助過我的人。



Contents

Abstract(Chinese)	i
Abstract(English)	ii
Acknowledgement.....	iii
Contents	iv
List of Figures	v
Chapter1 Introduction	1
Chapter2 Theories	5
2-1 Hartree approximation ¹⁰	5
2-2 Hartree-Fock approximation	6
2-3 Density Functional Theory.....	7
2-3-1 Hohenberg and Kohn theorem ¹¹	7
2-3-2 Kohn-Sham equation ¹²	9
(A) Pseudopotential Method.....	10
(B) Pseudopotential ¹⁵	12
(C) Local Density Functional Approximation	14
2-4 Band Theory	16
2-5 Phonon dispersion relation.....	18
2-5-1 Two atoms per primitive basis ²¹	18
2-5-2 Acoustic and optical phonon	20
2-5-3 Debye model for density of states.....	21
2-5-4 Phonon dispersion relation ²²⁻²⁴	22
2-5-5 Calculation of the force constant matrix	22
Chapter3 Calculation Method and Result	25
3-1 Crystal structures.....	25
3-2 VASP Calculation	30
3-3 Phonon dispersion relation.....	32
3-4 Matthiessen's rule ²⁵	37
3-5 Results and Discussion	40
3-5-1 Debye temperature calculation ^{27, 28}	40
3-5-2 Bloch-Gruneisen Model calculation	42
Chapter4 Conclusion	44
Chapter5 Reference	46

List of Figures

Fig. 1.1 The heat capacity of IrO_2 and RuO_2 ³	2
Fig. 1.2 Resistivity versus temperature of IrO_2 and RuO_2 ⁴	2
Fig. 1.3 The resistance as a function of temperature for different diameter in RuO_2 and IrO_2 ⁵	3
Fig. 3.1 The primitive cells for RuO_2 (upper panel) and IrO_2 (lower panel) in the rutile structures	27
Fig. 3.2 The structure of 1x1 nanowire for RuO_2 (upper panel) and IrO_2 (lower panel). The picture of the top-left corner is its bulk structure.	28
Fig. 3.3 The structure of 2x2 nanowire for RuO_2 (upper panel) and IrO_2 (lower panel).	29
Fig. 3.4 The contents of the POSCAR file.	30
Fig. 3.5 The partial contents of POTCAR file for local-density approximation.	31
Fig. 3.6 The contents of the KPOINTS file.	31
Fig. 3.7 The contents of the INCAR file.	32
Fig. 3.8 All output files of the VASP	32
Fig. 3.9 The contents of the INPHON file.	33
Fig. 3.10 The contents of the DISP file.	34
Fig. 3.11 The contents of the FORCES file.	35
Fig. 3.12 Phonon dispersion relation for the RuO_2 (upper panel) and IrO_2 (lower panel).	36
Fig. 3.13 The dependence of the Debye temperature in RuO_2 (upper panel) and IrO_2 (lower panel) on the diameters of the nanowires.	41
Fig. 3.14 The resistivity of RuO_2 (upper panel) and IrO_2 (lower panel) nanowires due to the interactions between electrons and the acoustic phonons.	43

Chapter1 Introduction

The rutile-structure transition-metal dioxides exhibit a variety of interesting physical properties that RuO_2 and IrO_2 have good conductivity properties and stability at high temperature. Their electrical transport properties are investigated for a long time, both experimentally and theoretically.

The electronic structures of RuO_2 and IrO_2 have been studied using the self-consistent semirelativistic linear muffin-tin-orbital (LMTO) method associated with the atomic sphere approximation in 1989 by J. H. Xu, T. Jarlborg and A. J. Freeman¹. Their results are in good agreement with experiments. In 1993, Keith M. Glassford and James R. Chelikowsky² have calculated the structures and electronic properties of RuO_2 using ab initio density functional theory with a fast iterative diagonalization technique with local-density-approximation (LDA) in a plane-wave basis and the pseudopotential.

In experiments, the heat capacities of RuO_2 and IrO_2 have been measured in 1969 by B. C. Passenheim and D. C. McCollum³. The heat-capacity measurements have been made by discontinuous heating method in a He cryostat. Their results show that $C = 0.059T^{-2} + 0.0225T^3 + 5.77T$ ($mJ / mole \cdot K$) for RuO_2 , and $C = 0.308T^{-2} + 0.0565T^3 + 5.51T$ ($mJ / mole \cdot K$) for IrO_2 . The experiment data is shown in figure 1.1.

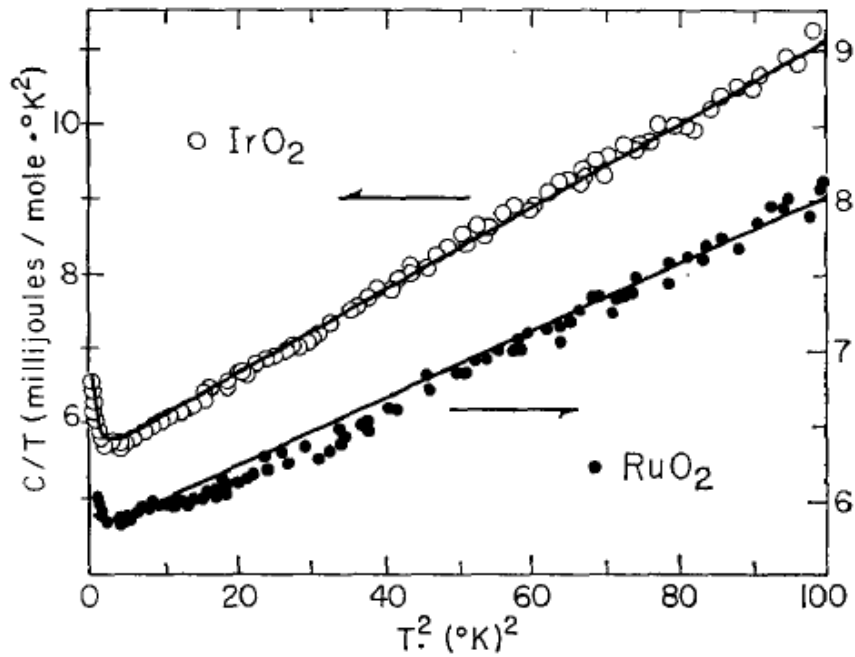


Fig. 1.1 The heat capacity of IrO_2 and RuO_2 ³.

W. D. Ryden and A. W. Lawson⁴ have measured the resistivity of RuO_2 and IrO_2 in the temperature range 4.2-1000 K in 1970. They have found the relation based on electron-electron and electron-phonon interband scatterings and fitted the temperature dependence of the resistivity. The figure 1.2 is the result of their experiment.

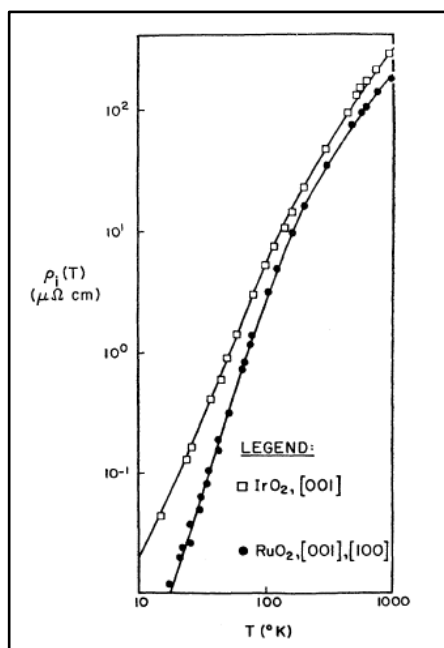


Fig. 1.2 Resistivity versus temperature of IrO_2 and RuO_2 ⁴.

In 2004, J. J. Lin, S M Huang, Y H Lin, H Liu, X X Zhang, R S Chen and Y S Huang^{5,6} firstly report their measurements of the resistivities and magnetoresistivities of RuO_2 and IrO_2 nanowires over a wide temperature range from 300 K down to 0.3 K .

Prof. Juhn-Jong Lin's group employs a thermal evaporation method to synthesize RuO_2 nanowires with controlled sizes. They control the sizes of the RuO_2 nanowires by adjusting the growth time and the average width of nanowires is about $\sim 90nm$. When they measure the transport properties of different diameters of nanowires, they find that the conductivities of the thick nanowires are better than the thin ones⁷. The results agree well with our ideal conjecture and we get the same relation in the theoretical calculation. In the figure 1.3, the resistivity varies with the temperature and they shift a constant in different diameters. The argument is similar for our results.

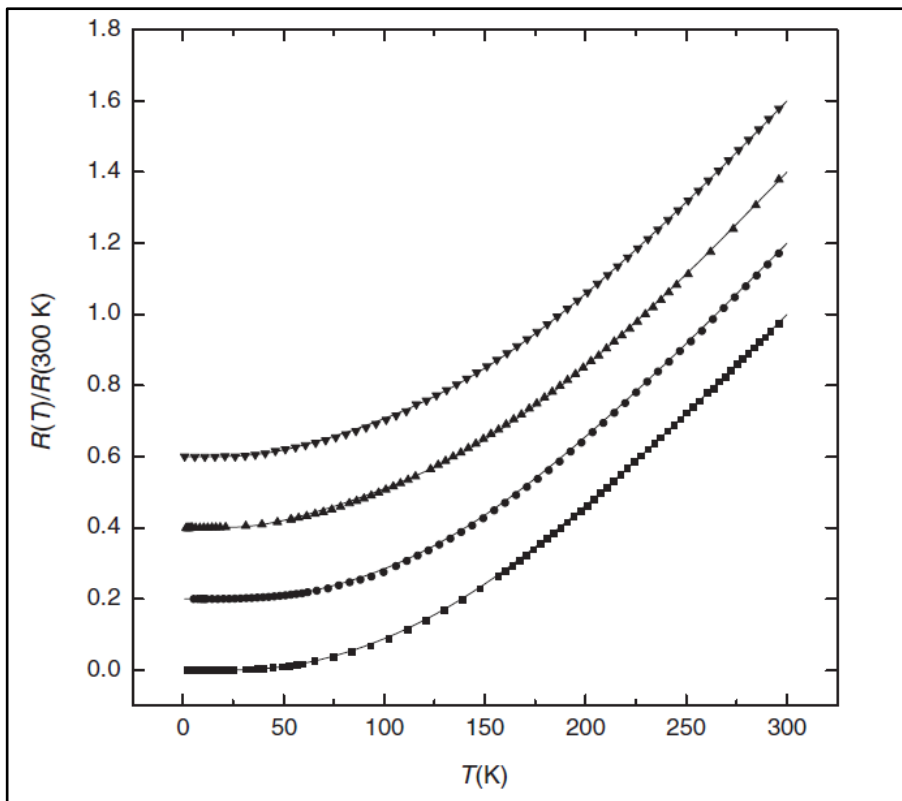


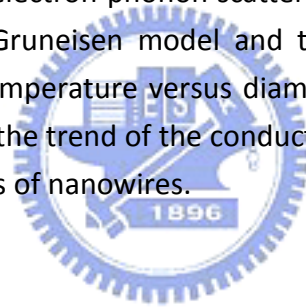
Fig. 1.3 The resistance as a function of temperature for different diameter in RuO_2 and IrO_2 ⁵.

Motivated by the above experiments, we theoretically investigate the dependence of the resistivity on the diameters of RuO_2 and IrO_2 nanowires in this work. We have calculated the Debye temperature of different diameters and compared the theoretical results with the experiments performed by Prof. Juhn-Jong Lin's group. We use Vienna Ab-initio Simulation Package (VASP)⁸ to relax the structures and the force constants of RuO_2 and IrO_2 bulk and nanowires. We also investigate the

phonon dispersion relation for RuO_2 and IrO_2 nanowires with different diameters, and the size effects on the electron transport according to the Bloch-Gruneisen equation.

The outline of the thesis is described as followings: first, we introduce the theories which we have applied to calculate the Debye temperature and resistivity in chapter 2. In section 2-1, we introduce the Hartree approximation; in section 2-2, we introduce the Hartree-Fock approximation; in section 2-3, we introduce the density functional theory (DFT); in section 2-4, we introduce the band theory; and in section 2-5, we introduce the phonon dispersion relation.

In chapter 3, we introduce the structures of RuO_2 and IrO_2 nanowires and the bulk crystals. We explained the parameters of VASP that is used to relax the structures of our systems. We also explain how to use "PHON"⁹ to obtain the phonon dispersion relations and the sound velocities. We also present the results of our calculations and discussion in the later part of the third chapter. According to the Matthiessen's rule with electron-phonon scatterings, we find the relation between the resistivity in the Bloch-Gruneisen model and the temperatures. We also study the relation of the Debye temperature versus diameters nanowires. Our objective is to theoretically investigate the trend of the conductivities and Debye temperatures as the function of the diameters of nanowires.



Chapter2 Theories

In this chapter we briefly introduce the theories of density functional theory and the theories of phonons. We introduce the Hartree and Hartree-Fock approximations in sections 2-1 and 2-2. In section 2-3, we introduce the density functional theory (DFT), which the ground state properties of a many electron system are uniquely determined by the electron density $n(r)$. In section 2-3-1, we introduce the Hohenberg and Kohn theorem. In section 2-3-2, we introduce the local density functional approximation (LDA) and the scheme of self-consistent calculations. In section 2-4, we briefly introduce the Bloch theorem and the band theory. In the section 2-5, we introduce the phonon dispersion relation and the phonon frequency from calculation the force constant matrices.

In many-electron system, the potential energies of electrons are complicated and the wave functions of many-electron system are difficult to solve. Density functional theory can simplify the calculations by mapping the complicated many-body wave functions into effective single-particle wave functions, where the effects of weak electron-electron interactions are included in the exchange-correlation energy.

2-1 Hartree approximation¹⁰

Consider the Hamiltonian of many-particle system with N electrons can be written as

$$H = \sum_i^N \frac{p_i^2}{2m} + V_{ext} + \frac{1}{2} \sum_i^N \sum_j^N \frac{e^2}{|r_i - r_j|}, \quad (2.1)$$

In the absence of the interaction between electrons, the many-body system will decouple into one-body problems. The ground-state wave function of the many-body system is expressed as the simple product of orthonormalized one-electron wave functions.

$$\Psi(r_1, r_2, \dots, r_N) = \psi_1(r_1)\psi_2(r_2) \dots \psi_N(r_N). \quad (2.2)$$

The total energy of the system is given by $E = \langle \Psi | H | \Psi \rangle$. By using the variational principle $\delta[E - \varepsilon_i \langle \psi_i | \psi_i \rangle] = 0$, where ε_i is the Lagrange multiplier with the

constraint $\langle \psi_i | \psi_j \rangle = \delta_{ij}$, the effective single-particle Schrodinger equation can be expressed as

$$\left[\frac{p^2}{2m} + V_{ext} + V_H \right] \psi_l = \epsilon_l \psi_l, \quad (2.3)$$

where $V_{ext} = -\sum_R \frac{Ze^2}{|\vec{r}_i - \vec{R}|}$. It describes an electron j at location \vec{r}_i of the ions in the potential field V_{ext} in the Coulomb potential of an average distribution of all other electrons. $V_H = \int d^3r' \frac{e^2}{|\vec{r} - \vec{r}'|} n_j(\vec{r}')$ is the Hartree potential corresponding to the electron-electron interactions. $n_j(\vec{r}) = \sum_j |\psi_j(\vec{r})|^2$ is the density of electrons.

The Eq.(2.3) is also called Hartree equation, and one can use the pseudopotential method to approximate the potential V_{ext} and the potential V_H .

2-2 Hartree-Fock approximation

Because the electrons are fermions, the total wave function is antisymmetric. To satisfy the Pauli Exclusion principle, one can extend the expression Eq.(2.2) as the Slater determinant of single particle wave functions:

$$\Psi = \frac{1}{\sqrt{N!}} \begin{vmatrix} \psi_1(r_1, s_1) & \psi_1(r_2, s_2) & \cdots & \psi_1(r_N, s_N) \\ \psi_2(r_1, s_1) & \psi_2(r_2, s_2) & \cdots & \vdots \\ \vdots & \vdots & \ddots & \vdots \\ \psi_N(r_1, s_1) & \cdots & \cdots & \psi_N(r_N, s_N) \end{vmatrix}, \quad (2.4)$$

where s denotes the electron spin.

By using the variational principle with the constraint $\langle \psi_i | \psi_j \rangle = \delta_{ij}$, Eq.(2.3) can be mapped into single particle pictures as followings:

$$\left[\frac{p^2}{2m} + V_{ext} + V_H + V_x \right] \psi_l = \epsilon_l \psi_l. \quad (2.5)$$

We see that Eq.(2.5) has one more term than Eq.(2.3) on left-hand side of the equal sign which is called exchange potential $V_x = -\sum_{j \neq i} \int d^3r' \psi_i^*(\vec{r}') \frac{e^2}{|\vec{r} - \vec{r}'|} \psi_j(\vec{r}')$.

The exchange potential V_x has the relations with Pauli Exclusion Principle and is a nonlocal potential. It can be calculated by using the local density functional approximation.

2-3 Density Functional Theory

The fundamental physical quantities in the ground state can be uniquely described from the electron density $n(\vec{r})$ in many-particle system. All ground state properties of the many electron system are functional of $n(\vec{r})$. In 1964 Hohenberg and Kohn prove that the ground state electron density uniquely determines the external potential. Kohn and Sham extended the theorem by separating the total energy into the kinetic energy of electron, the potential energy of attraction between electrons and nuclei, the coulomb potential energy of repulsion, and the exchange-correlation energy between electrons.

2-3-1 Hohenberg and Kohn theorem¹¹

The external potential is uniquely determined by the ground state electron density. The above theorem can be proved as follows :

We assume that two different potential V_1 and V_2 have the same $n(\vec{r})$.

Suppose $V_1 \neq V_2 + \text{constant}$ and $\Psi_1 \neq \Psi_2$ where Ψ_1 is the ground state wave function. The Schrodinger equation can be expressed as

$$H_1 \Psi_1 = E_1 \Psi_1$$

$$H_2 \Psi_2 = E_2 \Psi_2,$$

where E_1 and E_2 are eigen-energies of H_1 and H_2 , respectively.

With different external potentials, the Hamiltonian can be expressed as

$$H_1 = H_2 + V_1 - V_2.$$

Because $E_1 = \langle \Psi_1 | H_1 | \Psi_1 \rangle$ is the ground energy, we can obtain

$$\langle \Psi_1 | H_1 | \Psi_1 \rangle < \langle \Psi_2 | H_1 | \Psi_2 \rangle$$

$$E_1 < \langle \Psi_2 | H_2 | \Psi_2 \rangle + \langle \Psi_2 | V_1 - V_2 | \Psi_2 \rangle = E_2 + \int d^3r (V_1 - V_2) n(r), \quad (2.6)$$

and

$$E_2 < \langle \Psi_1 | H_1 | \Psi_1 \rangle + \langle \Psi_1 | V_2 - V_1 | \Psi_1 \rangle = E_1 + \int d^3r (V_2 - V_1) n(r). \quad (2.7)$$

Combine with Eq.(2.6) and Eq.(2.7), we obtain

$$E_1 - E_2 < \int d^3r (V_1 - V_2) n(r) < E_1 - E_2, \quad (2.8)$$

which leads to a contradiction and means that the assumptions are wrong. Thus, two different external potentials cannot correspond to the same non-degenerate ground state density. The total energy can be expressed as a functional of ground state charge density $n(\vec{r})$ in many-electron system.

$$E_{tot} = E_T[n].$$

If the charge density $n(\vec{r})$ is determined, all the ground state properties of the many-electron system will be determined.

2-3-2 Kohn-Sham equation¹²

From the Hohenberg and Kohn theorem, it is known that the ground state properties of many-particle system can be determined by the electron density $n(\vec{r})$. The charge density in the ground state can be solved iteratively until the self-consistent is achieved.

The ground state energy of a homogeneous interacting electron gas can be written as

$$E_T[n] = T[n] + \int V_{ext}(\vec{r})n(\vec{r})d^3r + \frac{1}{2} \iint \frac{n(\vec{r})n(\vec{r}')}{|\vec{r}-\vec{r}'|} d^3r d^3r' + E_{xc}[n]. \quad (2.9)$$

In the right-hand side, the first term is the kinetic energy as a functional of non-interacting electrons with density $n(\vec{r})$; the second term is external potential energy relative to electrons; the third term is Coulomb energy between electrons; and the fourth term is the exchange-correlation energy functional of an interacting system with density $n(\vec{r})$. By the variational principle with the total electron $N = \int n(\vec{r})d^3r$ for the ground state, one has

$$\frac{\delta T[n]}{\delta n} + V_{ext}(\vec{r}) + \int \frac{n(\vec{r}')}{|\vec{r}-\vec{r}'|} d^3r' + V_{xc}(\vec{r}) = \mu, \quad (2.10)$$

where $V_{xc}[\vec{r}] = \frac{\delta E_{xc}[n]}{\delta n}$ and $V_H = \int \frac{n(\vec{r}')}{|\vec{r}-\vec{r}'|} d^3r'$ μ is Lagrange parameter.

In the absence of the exchange-correlation potential, it goes back to Hartree approximation. Comparing Eq.(2.10) with Eq.(2.5), it is regarded as an effective potential of the single-electron wave equation which is called Kohn-Sham Equation.

$$\left[-\frac{\hbar^2}{2m} \nabla^2 + V_{ext}(\vec{r}) + V_H(\vec{r}) + V_{xc}(\vec{r}) \right] \psi_i(\vec{r}) = \epsilon_i \psi_i(\vec{r}), \quad (2.11)$$

$E_{xc}[n]$ is the exchange and correlation energy of an interacting system with density $n(\vec{r})$.

(A) Pseudopotential Method

The early calculations of first-principles pseudopotential are made within the scheme of orthogonalized-plane-wave (OPW) atomic calculation. The wave functions in this way exhibit the correct shape outside the core region; however, they differ from the real wave functions by a normalization factor¹³. Hamann, Schluter and Chiang¹⁴ (HSC) propose a model pseudopotential to solve the problems that have four properties : (1) real and pseudo valence eigenvalues agree for a chosen atomic configuration; (2) real and pseudo wave functions agree beyond a chosen core radius r_c ; (3) the integrals from 0 to r of the real and pseudo charge densities agree for $r > r_c$ for each valence state, this is norm conservation condition; (4) The logarithmic derivatives of the real and pseudo wave function and their first energy derivatives agree for $r > r_c$.

Because the lattice has the periodic characteristic, the wave functions must satisfy the Bloch theorem. It can be written as expansion of the following form:

$$\Psi_{nk}(\vec{r}) = \sum_G \alpha_G^{nk} \frac{1}{\sqrt{\Omega}} e^{i(\vec{k}+\vec{G})\cdot\vec{r}}. \quad (2.12)$$

In the pseudopotential method, the pseudopotential V_{ps} is constructed on the valence electrons and the core electrons have been transformed away. The pseudo-Hamiltonian of the valence electrons can be expressed as

$$H = \frac{p^2}{2m} + V_{ps} + V_H + V_{xc}, \quad (2.13)$$

where

$$V_{ps} = \sum_{\vec{R}} V_{ion}(\vec{r} - \vec{r}_j - \vec{R}).$$

$V_{ion}(\vec{r})$ is non-local potential and it is relation to the angular momentum l . The

angular momentums of the electron in the s, p and d orbitals are 0, 1 and 2, respectively. The potential can be expressed as

$$V_{ion}(\vec{r}) = \sum_{i=0}^2 V_i(\vec{r}) \hat{P}_i. \quad (2.14)$$

\hat{P}_i is the projection operator of the angular momentum. The Hartree potential satisfies the Poisson equation and it can be written as

$$\nabla^2 V_H(\vec{r}) = -8\pi n(\vec{r}). \quad (2.15)$$

$n(\vec{r})$ is the density of the pseudo valence electrons and the V_{xc} can be regarded as functional of $n(\vec{r})$ from LDA. We define the elements of the matrix S that

$$S_{\vec{G}, \vec{G}'}^k = \langle \vec{k} + \vec{G}' | \vec{k} + \vec{G} \rangle = \delta_{\vec{G}, \vec{G}'}. \quad (2.16)$$

The pseudopotentials of the ion V_{ion} can be separated into local and non-local potential ($V_{ion} = V_{ion}^{loc} + V_{ion}^{nl}$). The V_H and V_{xc} are functional of $n(\vec{r})$ that are also local potential. The Hamiltonian can be rewritten as

$$H = T + V^{loc} + V^{nl} \quad T = \frac{p^2}{2m}, \quad (2.17)$$

$$\langle \vec{k} + \vec{G}' | T | \vec{k} + \vec{G} \rangle = |\vec{k} + \vec{G}|^2 \delta_{\vec{G}, \vec{G}'}, \quad (2.18)$$

$$\langle \vec{k} + \vec{G}' | V^{loc} | \vec{k} + \vec{G} \rangle = V^{loc}(\vec{G} - \vec{G}'), \quad (2.19)$$

$$\langle \vec{k} + \vec{G}' | V^{nl} | \vec{k} + \vec{G} \rangle = V^{nl}(\vec{k} + \vec{G}', \vec{k} + \vec{G}). \quad (2.20)$$

(B) Pseudopotential¹⁵

Pseudopotentials are introduced to simplify electronic structure calculations by eliminating the need to atomic core states and the strong potentials responsible for binding them.

To construct atomic pseudopotential φ_{lm} at a given energy which are identical to atomic eigenfunctions. The φ_{lm} are continued inside r_c with the condition that $\varphi_{lm} \rightarrow r^l$ for $r \rightarrow 0$ and with the norm-conserving condition, one has

$$\int_0^{r_c} \varphi_{lm}^2 d^3r = \int_0^{r_c} \psi_{lm}^2 d^3r, \quad (2.21)$$

The pseudopotentials are obtained by inverting the Schrodinger equation

$$V_l(r) = [\nabla_r^2 \varphi_l] / \varphi_l + E - \frac{l(l+1)}{r^2}. \quad (2.22)$$

The complete pseudopotential is then written as

$$V_{PS} = V_{loc} + V_{non} = V_{loc}(r) + \sum_{lm} |Y_{lm}(\theta\varphi)\rangle \delta v_l \langle Y_{lm}(\theta\varphi)|, \quad (2.23)$$

where $\delta v_l = 0$ for $r > r_c$ and V_{loc} is the local potential and is an arbitrary function for $r < r_c$. The semilocal form¹⁶ (i.e. nonlocal in angular coordinates but local in radial coordinate) of the Hamman-Schluter-Chiang (HSC) pseudopotential which used in an expansion of N plane waves requires the evaluation of $\frac{N(N+1)}{2}$ integral for each δv_l . The nonlocal form can be introduced,

$$V_{ps} = V_{loc} + \sum_{lm} |\varphi_{lm}(r)\delta v_l(r)\rangle B_l^{-1} \langle \varphi_{lm}(r)\delta v_l(r)|, \quad (2.24)$$

where

$$B_l = \langle \varphi_{lm} | \delta v_l | \varphi_{lm} \rangle.$$

Vanderbilt generalized Eq.(2.24) with $\varphi_i(r)$ and $\delta v_i(r)$ where the i subsumes

the l, m and also includes two or more energies at which the $\varphi_{lm}(r)$ are evaluated. This result in B_l becoming a matrix

$$B_{ij} = \langle \varphi_i | \delta v_j | \varphi_j \rangle,$$

which is not Hermitian and the generalized norm-conservation requirement,

$$Q_{ij} = \int_0^{r_c} Q_{ij}(r) d^3 r = \int_0^{r_c} [\psi_i^*(r) \psi_j(r) - \varphi_i^*(r) \varphi_j(r)] d^3 r = 0, \quad (2.25)$$

and Vanderbilt¹⁷ defines

$$|\beta_i\rangle = \sum_j (B^{-1})_{ji} |\delta v_j \varphi_j\rangle, \quad (2.26)$$

which is substituted into the Eq.(2.24) and one can obtain the pseudopotential

$$V_{ps} = V_{loc} + \sum_{i,j} |\beta_i\rangle B_{ij} \langle \beta_j|. \quad (2.27)$$

In general, it is difficult to apply Eq.(2.25), results in φ_{lm} whose plane-wave expansions are extremely slowly converging. To avoid applying Eq.(2.25), Chou¹⁸ constructed norm-conserving φ_{nlm} at two energies E_n and inverted the Schrodinger equation to obtain their δv_{nl} which she averaged to obtain $\delta \bar{v}_l$, yielding

$$V_{ps} = V_{loc}(r) + \sum_{nlm} |\bar{\varphi}_{rlm}(r) \delta \bar{v}_l(r)\rangle A_{nl}^{-1} \langle \bar{\varphi}_{rlm}(r) \delta \bar{v}_l(r)|, \quad (2.28)$$

where

$$A_{nl} = \langle \bar{\varphi}_{nlm} | \delta \bar{v}_n | \bar{\varphi}_{nlm} \rangle.$$

The A_{nl} is Hermitian and the $\bar{\varphi}_{nlm}(r)$ are solutions of the pseudo Schrodinger equation at E_n with δv_{nl} replaced by $\delta \bar{v}_l$.

(C) Local Density Functional Approximation

The exchange-correlation energy is relation to the electronic distribution in the system. It is difficult to give an exact expression for E_{xc} because of its complexity. In order to simplify this complexity, Kohn and Sham suggested using the homogeneous electron gas system to approximate the energy contribution from $E_{xc}[n]$ in 1965. If the electronic density varies slowly, the exchange-correlation functional can be written as

$$E_{xc}[n] = \int \varepsilon_{xc}[n](\vec{r}) d^3r, \quad (2.29)$$

where the exchange-correlation potential can be expressed as

$$V_{xc}(\vec{r}) = \frac{\delta E_{xc}[n]}{\delta n} = \frac{d}{dn} \{n\varepsilon_{xc}(n)\}, \quad (2.30)$$

where $\varepsilon_{xc}[n]$ is the exchange-correlation energy density of the homogeneous electron gas. $V_{xc}(n)$ is the exchange and correlation contribution to the chemical potential of a homogeneous gas of density n .

The exchange-correlation energy density¹⁹ can be separated into $\varepsilon_x[(\vec{n})]$ and $\varepsilon_c[(\vec{n})]$. $\varepsilon_x[(\vec{n})]$ is the exchange energy of a homogeneous electron gas and $\varepsilon_c[(\vec{n})]$ is the correlation energy of a homogenous electron gas.

Within Hartree-Fock approximation the exchange energy density can be obtained by solving the Schrodinger equation of the non-interacting homogenous electron gas.

$$\varepsilon_x(\vec{r}) = \frac{-0.458}{r_s} \quad r_s \text{ is Wigner-Seitz radius,}$$

$$\text{where } n(\vec{r}) = \left(\frac{4}{3}\pi r_s^3\right)^{-1} \Rightarrow \varepsilon_x(\vec{r}) = -0.458 \left(\frac{4}{3}\pi n(\vec{r})\right)^{\frac{1}{3}}. \quad (2.31)$$

From the Eq.(2.31), we can know that the exchange energy density $\varepsilon_x(\vec{r})$ is proportion to the electron density $n(\vec{r})$ to the power of one third.

An approximation of the correlation energy is based on Quantum Monte Carlo calculations by Ceperley and Alder²⁰. The wave function for electrons in a finite volume subject to periodic boundary conditions and extrapolated the energy per electron to infinite volume. The Ceperley's parameterization of the correlation energy for $r_s \geq 1$ is

$$\varepsilon_c(\bar{r}) = \frac{r_s}{1 + \beta_1 \sqrt{r_s} + \beta_2 r_s} = \frac{-0.1423}{1 + 1.0529 \sqrt{r_s} + 0.3334 r_s}, \quad (2.32)$$

the high-density form of ε_c ($r_s < 1$) is

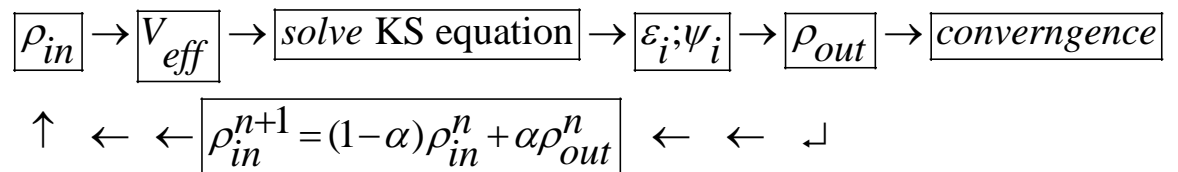
$$\varepsilon_c(\bar{r}) = 0.0311 \ln r_s - 0.048 + 0.002 r_s \ln r_s - 0.0116 r_s$$

Substituting Eq.(2.31) into Eq.(2.30), the relation between exchange-correlation potential and electronic density can be expressed as

$$V_{xc} = \left[1 - \frac{r_s}{3} \frac{d}{dr_s} \right] \varepsilon_{xc}. \quad (2.33)$$

In many-electron system, we give the initial data of the electronic density to calculate the potential each term, and get the effective potential V_{eff} to solve the solution of the Kohn-Sham equation. The wave function is obtained by Kohn-Sham equation and the new electronic density is calculated from the wave function. If the difference in value between the new electronic density and the initial electronic density is too big, they will be mixed to generate another electronic density, and repeat the above procedures until the difference in value between the new density and last density is very small. The above procedures are called self-consistent procedure.

The convergence of the flow chart :



2-4 Band Theory

The solutions of the Schrodinger equation for a periodic potential by Bloch theorem can be expressed as

$$\psi_k(\vec{r}) = e^{i\vec{k}\cdot\vec{r}} u_k(\vec{r}), \quad (2.34)$$

where $u_k(\vec{r})$ has the period of the crystal lattice with $u_k(\vec{r}) = u_k(\vec{r} + \vec{R})$.

We substitute Eq.(2.34) into the Kohn-Sham equation

$$\left[-\frac{\hbar^2}{2m} \nabla^2 + V_{ext}(\vec{r}) + V_H(\vec{r}) + V_{xc}(\vec{r}) \right] \psi_k(\vec{r}) = \varepsilon_k \psi_k(\vec{r}), \quad (2.35)$$

here

$$\begin{aligned} -\frac{\hbar^2}{2m} \nabla^2 \psi_k(\vec{r}) &= -\frac{\hbar^2}{2m} \nabla[\nabla e^{i\vec{k}\cdot\vec{r}} u_k(\vec{r})] = -\frac{\hbar^2}{2m} \nabla[e^{i\vec{k}\cdot\vec{r}} (i\vec{k}u_k + \nabla u_k(\vec{r}))] \\ &= -\frac{\hbar^2}{2m} e^{i\vec{k}\cdot\vec{r}} [i\vec{k} + \nabla]^2 u_k(\vec{r}), \end{aligned}$$

The Kohn-Sham equation is rewritten as

$$H_k u_k(\vec{r}) = \varepsilon_k u_k(\vec{r}),$$

$$\text{where } H_k = -\frac{\hbar^2}{2m} [i\vec{k} + \nabla]^2 + V_{ext}(\vec{r}) + V_H(\vec{r}) + V_{xc}(\vec{r}).$$

This is a partial differential equation with complicate boundary condition. One can reduce this complicate boundary value problem to a simple matrix diagonalization problem using Rayleigh-Ritz variational principle.

We choose a basis function $\chi_n(\vec{r})$,

$$\text{where } \chi_n(\vec{r} + \vec{R}) = \chi_n(\vec{r}),$$

$$\text{and } u_k(\vec{r}) = \sum_n C_n \chi_n(\vec{r}). \quad (2.36)$$

According to the variational principle, we know that the expectation value of the Hamiltonian by the arbitrary wave function must be greater than ground-state energy of the system.

$$\langle u_k | H | u_k \rangle \geq E_{GS},$$

or

$$\langle u_k | H | u_k \rangle - E_{GS} \langle u_k | u_k \rangle \geq 0. \quad (2.37)$$

If one can find out the minimum eigenvalue of the system, one will get the energy close to the ground-state energy. We substitute Eq.(2.36) into Eq.(2.37) with the equal sign the variational principle tell us that in the ground state

$$\frac{\partial}{\partial C_l^*} \left\langle \sum_n C_n \chi_n | H_k | \sum_m C_m \chi_m \right\rangle - \lambda \frac{\partial}{\partial C_l^*} \left\langle \sum_n C_n \chi_n | \sum_m C_m \chi_m \right\rangle = 0,$$

then

$$\frac{\partial}{\partial C_l^*} \sum_n \sum_m C_n^* C_m H_{nm}(k) - \lambda \frac{\partial}{\partial C_l^*} \sum_n \sum_m C_n^* C_m S_{nm} = 0.$$

More compactly one may write in this way.

$$\sum_m H_{lm}(k) C_m - \lambda \sum_m S_{lm} C_m = 0$$

$$\Rightarrow \underset{\sim}{H} \underset{\sim}{C} - \lambda \underset{\sim}{S} \underset{\sim}{C} = 0, \quad (2.38)$$

where $H_{nm}(k) = \langle \chi_n | H_k | \chi_m \rangle$ and $S_{nm} = \langle \chi_n | \chi_m \rangle$.

If the matrices H_{nm} and S_{nm} are given, the wave functions can be obtained by diagonalizing. The different bases lead to different approximations, for example, APW,

LPAW, LCAO, etc.

2-5 Phonon dispersion relation

A phonon is a quantized mode of vibration occurring in a rigid crystal lattice.

2-5-1 Two atoms per primitive basis²¹

Consider the elastic vibrations of a crystal which is correlated to displacements of other atoms nearby. Most simple situation is obtained in the [100], [110] and [111] propagation directions of cubic crystals. If a wave is propagating along one of these directions entire planes of atoms move in phase with displacements either parallel (longitudinal) or perpendicular (transverse) to the direction of the wave vector \vec{K} .

Here we think about two different atoms per primitive basis. Atom 1 with mass M_1 is displaced by u_{s-1}, u_s, u_{s+1} and atom 2 with mass M_2 is displaced by v_{s-1}, v_s, v_{s+1} , where $M_1 > M_2$. The force constant is C and force between two different neighboring atoms is $F = C(v_s - u_s)$ from Hooke's law. The equation of motion is



$$M_1 \frac{d^2 u_s}{dt^2} = C(v_s + v_{s-1} - 2u_s) \quad (2.39)$$

$$M_2 \frac{d^2 v_s}{dt^2} = C(u_{s+1} + u_s - 2v_s).$$

The solution in the form of a traveling wave with different amplitude u, v can be written as

$$u_s = u e^{i(sKa - \omega t)}$$

$$v_s = v e^{i(sKa - \omega t)}, \quad (2.40)$$

where the lattice constant a is defined as between nearest identical planes, not nearest-neighbor planes. Substitute Eq.(2.40) into Eq.(2.39) and we can get

$$-\omega^2 M_1 u = Cv(1 + e^{-iKa}) - 2Cu$$

$$-\omega^2 M_2 v = Cu(e^{iKa} + 1) - 2Cv, \quad (2.41)$$

Transform the above equation to another type

$$\begin{aligned} (2C - \omega^2 M_1)u - C(1 + e^{-iKa})v &= 0 \\ -C(e^{iKa} + 1)u + (2C - \omega^2 M_2)v &= 0, \end{aligned} \quad (2.42)$$

The solution of the phonon dispersion relation can be found by the determinant of the coefficients of above equation:

$$\det \begin{vmatrix} 2C - \omega^2 M_1 & -C(1 + e^{-iKa}) \\ -C(e^{iKa} + 1) & 2C - \omega^2 M_2 \end{vmatrix} = 0, \quad (2.43)$$

here

$$M_1 M_2 \omega^4 - 2C(M_1 + M_2)\omega^2 + 2C^2(1 - \cos Ka) = 0,$$

and it is known $\cos Ka = 1 - \frac{(Ka)^2}{2!} + \frac{(Ka)^4}{4!} - \dots \approx 1 - \frac{(Ka)^2}{2!}$ when $Ka \ll 1$

$$\begin{aligned} \omega^2 &= \frac{2C(M_1 + M_2) \pm \sqrt{4C^2(M_1 + M_2)^2 - 4M_1 M_2 C^2 (Ka)^2}}{2M_1 M_2} \\ &= \frac{2C(M_1 + M_2) \pm \{2C(M_1 + M_2)[1 - \frac{M_1 M_2}{M_1 + M_2} (Ka)^2]^{\frac{1}{2}}\}}{2M_1 M_2}, \end{aligned} \quad (2.44)$$

then $(1+x)^{1/2} \approx 1 + \frac{1}{2}x$ when $x \ll 1$ and the above equation is similar

$$\omega^2 = \frac{C(M_1 + M_2) \pm \{C(M_1 + M_2)[1 - \frac{M_1 M_2}{2(M_1 + M_2)^2} (Ka)^2]\}}{M_1 M_2}. \quad (2.45)$$

We can get the two solutions of the Eq.(2.45).

$$\omega^2 = 2C\left(\frac{1}{M_1} + \frac{1}{M_2}\right), \quad (2.46)$$

$$\omega^2 = \frac{C}{2(M_1 + M_2)}(Ka)^2, \quad (2.47)$$

where Eq.(2.46) is called optical branch and Eq.(2.47) is called acoustical branch. For first Brillouin zone the boundary condition is $-\frac{\pi}{a} < K < \frac{\pi}{a}$. At $K_{\max} = \pm \frac{\pi}{a}$ we can get the solution

$$\omega^2 = \frac{2C}{M_2} \quad \text{for optical mode}$$

$$\omega^2 = \frac{2C}{M_1} \quad \text{for acoustical mode}$$

2-5-2 Acoustic and optical phonon

It is mentioned before that there are two types of phonons: acoustic phonon and optical phonon in solid with more than one atom in the smallest unit cell.

The acoustic phonons which are the phonons described above and have frequencies that become small at the long wavelengths, and correspond to sound waves in the lattice.

The optical phonons, which also arise in crystals with more than one atom in the smallest unit cell, always have some minimum frequency of vibration, even when their wavelength is large. They are called optical because in ionic crystals (like sodium chloride) they can be excited by light (in fact, infrared radiation). Optical phonons that interact in this way with light are called infrared active. Optical modes correspond to a vibration where the positive and negative ions at adjacent lattice sites swing against each other, creating a time-varying electrical dipole moment.

If there are p atoms in the primitive cell, there are $3p$ branches to the dispersion relation : 3 acoustical branches and $3p - 3$ optical branches. For example, germanium have two atoms in the primitive cell, have six branches : one LA (longitudinal acoustical) , one LO (longitudinal optical) , two TA (transverse acoustical) and two LA (longitudinal acoustic).

There are N primitive cells with p atoms in the primitive cell so there are pN atoms. Thus the LA and two TA branches have total of $3N$ modes, thereby

accounting for $3N$ of the total degrees of freedom. The remaining $(3p-3)N$ degrees of freedom are accommodated by the optical branches.

2-5-3 Debye model for density of states

We apply periodic boundary conditions over N^3 primitive cells and consider a cube with length L . The total number of states in K space with the volume of a sphere of radius K :

$$N = \left(\frac{L}{2\pi}\right)^3 \left(\frac{4\pi K^3}{3}\right) \quad (2.48)$$

The density of state for each polarization is

$$D(\omega) = \frac{dN}{d\omega} = \left(\frac{VK^2}{2\pi^2}\right) \left(\frac{dK}{d\omega}\right) \quad (2.49)$$

In the Debye approximation the dispersion relation is written as

$$\omega = \nu K \quad (2.50)$$

where ν is the velocity of the sound. Substitution Eq.(2.50) into Eq.(2.49), the density of states becomes

$$D(\omega) = \frac{V\omega^2}{2\pi^2\nu^3} \quad (2.51)$$

A cutoff frequency ω_D is determined by Eq.(2.49) as

$$\begin{aligned} \omega_D^3 &= \nu^3 K_D^3 \\ &= \frac{6\pi^2 \nu^3 N}{V} \end{aligned} \quad (2.52)$$

The Debye temperature Θ_D in terms of ω_D is defined as

$$\Theta_D \equiv \frac{\hbar\omega_D}{k_B} = \frac{\hbar\nu}{k_B} \cdot \left(\frac{6\pi^2 N}{V}\right)^{\frac{1}{3}} \quad (2.53)$$

2-5-4 Phonon dispersion relation²²⁻²⁴

We apply the code “PHON” to calculate the force constant matrices and phonon frequency in crystals. “PHON” is an open source code, developed by Dario Alfe. The phonon dispersion relations have been calculated using ab-initio force constant method using the VASP program.

The central quantity in the calculations of the phonon frequencies is the force-constant matrix $\Phi_{is\alpha,jt\beta}$. The force constant matrices are calculated in terms of Hellmann-Feynman forces by the displacement of a single atom in the frame work of self-consistent density functional theory calculations in the local density approximation.

The frequencies at wave vector k are the eigenvalues of the dynamical matrix

$D_{s\alpha,t\beta}$, defined as

$$D_{s\alpha,t\beta}(k) = \frac{1}{\sqrt{M_s M_t}} \sum_i \Phi_{is\alpha,jt\beta} e^{ik \cdot (R_{jt} - R_{is})}, \quad (2.54)$$

where the atoms s, t are in the primitive cell i, j , α and β are Cartesian components, R_{is} is the position of atom s in the primitive i , and the M_s and M_t are the masses of the atom s and t respectively. If the force constant matrix is known, the frequencies ω_{ks} can be obtained at any wave vector k . In principle, the elements of $\Phi_{is\alpha,jt\beta}$ are nonzero for arbitrarily large separations $|R_{jt} - R_{is}|$, but they decay rapidly with separation, so that a key issue in achieving a fixed target precision is the cut-off distance beyond which the elements can be neglected.

2-5-5 Calculation of the force constant matrix

We calculate the force constant matrix using the small-displacement method which atom s is displaced by a vector $u_{is\alpha}$ and the force F is given

$$F_{is\alpha} = - \sum_{jt\beta} \Phi_{is\alpha,jt\beta} u_{jt\beta}, \quad (2.55)$$

and the force constant matrix can be written as

$$\Phi_{is\alpha, jt\beta} = -\frac{F_{is\alpha}}{u_{jt\beta}}. \quad (2.56)$$

The elements of $\Phi_{is\alpha, jt\beta}$ are obtained from given $jt\beta$ by introducing a small displacement $u_{jt\beta}$ and all other displacements are zero.

The entire force constant matrix is obtained by making three independent displacements for each atom in the primitive cell. As a result, it has to move $3N$ times per primitive cell. Usually, the number of movements is reduced by atom symmetry. Because the $\Phi_{is\alpha, jt\beta}$ in the formula for $D_{s\alpha, t\beta}(k)$ is the force constant matrix in the infinite lattice with no restriction on the wave vector k , it is impossible to extract the infinite-lattice $\Phi_{is\alpha, jt\beta}$ from supercell calculations. In order to solve this question, it must need an assumption. The assumption is that the infinite-lattice $\Phi_{is\alpha, jt\beta}$ vanishes when the separation $R_{jt} - R_{is}$ is such that the positions R_{is} and R_{jt} lie in different Wigner-Seitz (WS) cells of the chosen superlattice. If it take the WS cells centered on R_{jt} , then the infinite-lattice value of $\Phi_{is\alpha, jt\beta}$ vanishes if R_{is} is in a different WS cell; it is equal to the supercell value if R_{is} is in the same WS cell. With this assumption, the $\Phi_{is\alpha, jt\beta}$ elements will converge to the correct infinite-lattice values as the dimensions of the supercell are systematically increased.

We displace the atom one in the primitive cell and calculate the force induced by the displacement of the other atoms. Then we displace the atom two to calculate the induced force and repeat above procedure until the set of displacement vectors is complete. Not all atoms should be displaced to calculate their induced forces. The calculations can be reduced if there is a symmetry operation S in the system. For example, we will not displace the atom two if the crystal is unchanged according to symmetry operator S which transforms atom two into atom one.

The part of force constant matrix associated with its displacement vectors can be calculated using

$$\Phi_{is,02} = B(S)\Phi_{\lambda_{is}(S),01}B(S^{-1}), \quad (2.57)$$

where $B(S)$ is the 3x3 matrix representing the point group part of S in Cartesian coordinates and $\lambda_{is}(S)$ indicates the atom of the crystal. If the application of all symmetry operations does not create a set of three linear independent displacement vectors on all atoms of the basis, it will create another displacement vector $u'_{j1\beta}$ which is linear dependent with the first one and perform a new total energy calculation and execute again the same operations.

It is worth noting how to choose the displacement vectors of atoms for the force constant matrices. If the displacements are too small, then the forces induced may be smaller than the limit of the accuracy in the calculations. Thus, one needs to choose appropriate displacement vectors of atoms. Conventionally, it can be chosen according to the certain percentage of the nearest-neighbor distant in normal case.



Chapter3 Calculation Method and Result

The electronic structures and electrical transport properties of the dioxides RuO_2 and IrO_2 have been extensively studied recently.

In experiment, the heat capacities of RuO_2 and IrO_2 have been measured in 1969 by B. C. Passenheim and D. C. McCollum. W. D. Ryden and A. W. Lawson have measured the resistivity of RuO_2 and IrO_2 in the temperature range from 4.2 to 1000 K in 1970.

In 2004, J. J. Lin, S M Huang, Y H Lin, H Liu, X X Zhang, R S Chen and Y S Huang have reported their measurements of the resistivities and magnetoresistivities of several RuO_2 and IrO_2 nanowires over a wide temperature range from 300 K down to 0.3 K. Motivated by this experiment, we theoretically investigate the transport properties of RuO_2 and IrO_2 nanowires. The theoretical calculation of RuO_2 and IrO_2 nanowires are based on the density functional theory within local density approximation.

3-1 Crystal structures

Ruthenium dioxide crystallizes in the rutile structure with space-group symmetry $P4_2/mnm (D_{4h}^{14})$, as is common in the iridium dioxide. The tetragonal Bravais lattice contains two RuO_2 and IrO_2 molecules per primitive cell. The metal atoms, placed at the cell corner and body center, are nearly octahedrally coordinated by oxygen atoms.

For the RuO_2 bulk, the lattice parameters are $a=b=4.56 \text{ \AA}$, $c=3.16 \text{ \AA}$ in theoretical calculation which are in good agreement with the experimental values, $a=b=4.500\pm 0.005 \text{ \AA}$, $c=3.101\pm 0.006 \text{ \AA}$. Similarly in the case of the IrO_2 bulk material, the lattice parameters for theoretical value are $a=b=4.49 \text{ \AA}$, $c=3.15 \text{ \AA}$ which is in good agreement with the experimental values: $a=b=4.518 \text{ \AA}$, $c=3.165 \text{ \AA}$. The two Ru and

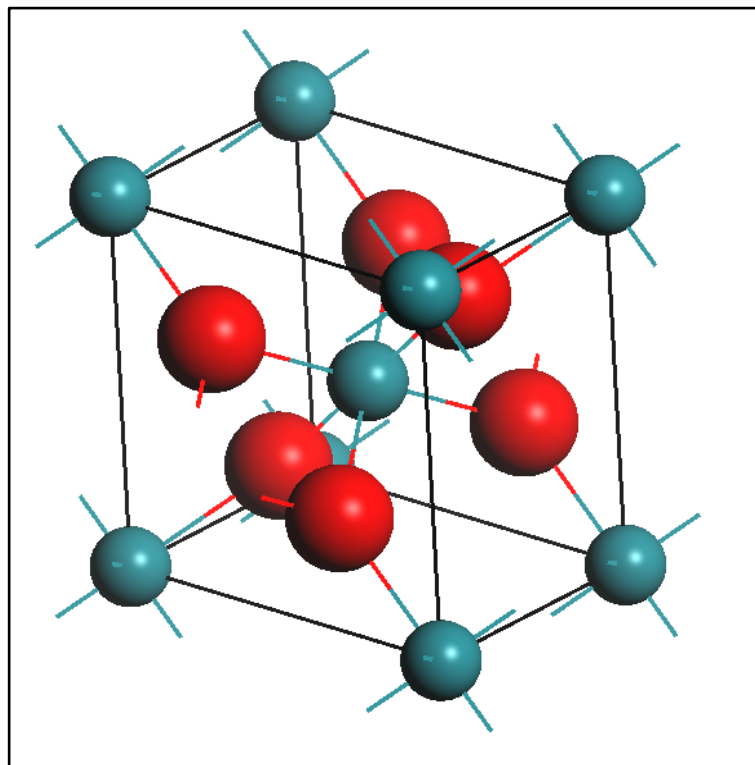
Ir atoms occupy the sites, $(0,0,0; \frac{1}{2}, \frac{1}{2}, \frac{1}{2})$, and the four O atoms occupy the sites, $\pm(u, u, 0; u + \frac{1}{2}, \frac{1}{2} - u, \frac{1}{2})$, where u is an internal parameter and along with a and c/a

describe the oxygen octahedral surrounding each Ru and Ir atom. We summarize the lattice parameters a , c , c/a and u for the RuO_2 and IrO_2 in the Table 1.

Property	(RuO ₂) Theory	Experiment	(IrO ₂) Theory	Experiment
a (Å)	4.56	4.492	4.49	4.518
c (Å)	3.16	3.106	3.15	3.165
c/a	0.694	0.692	0.702	0.698
u	0.3068	0.3058	0.25	0.25

TABLE 1. Comparison of structural parameters for the RuO_2 and IrO_2 in the rutile structure obtained from the experimental measurements and the theoretical calculations².

We show the structures of RuO_2 and IrO_2 in Fig. 3.1.



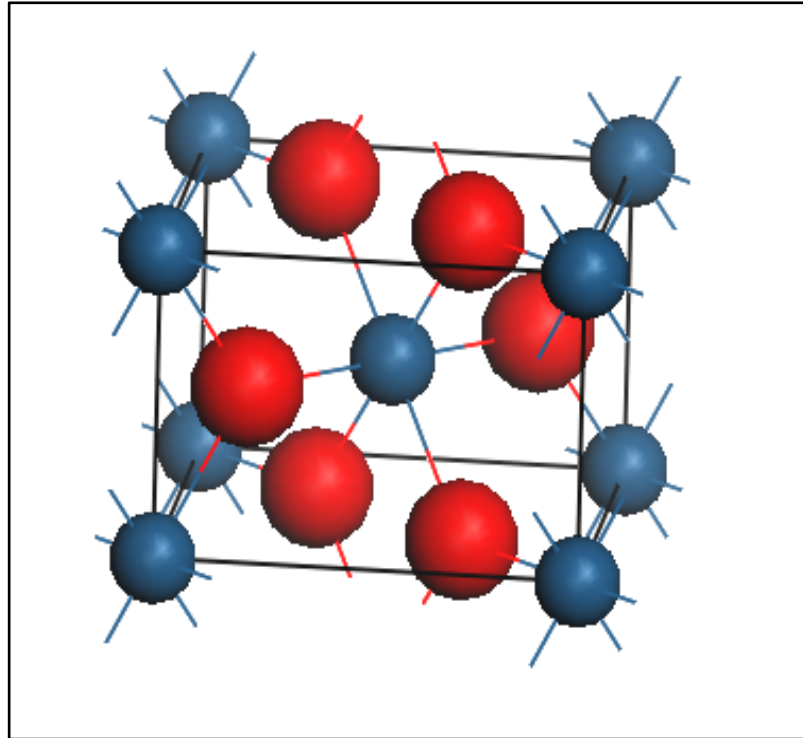


Fig. 3.1 The primitive cells for RuO_2 (upper panel) and IrO_2 (lower panel) in the rutile structures.

For the bulk the primitive cell is periodic permutation in the x, y and z direction. We then build up the 1x1 and 2x2 nanowires along the (001) direction from the structure of the bulk crystal. It has the same periodicity along the z direction for 1x1 nanowires. The periodic permutation for 1x1 nanowires is one primitive cell and two empty primitive cells along the x and y direction. Thus, the lattice parameters become $a=b=13.68 \text{ \AA}$, $c=3.16 \text{ \AA}$ for the RuO_2 and $a=b=13.47 \text{ \AA}$, $c=3.15 \text{ \AA}$ for the IrO_2 . The structure of 1x1 nanowires is shown in Fig. 3.2.

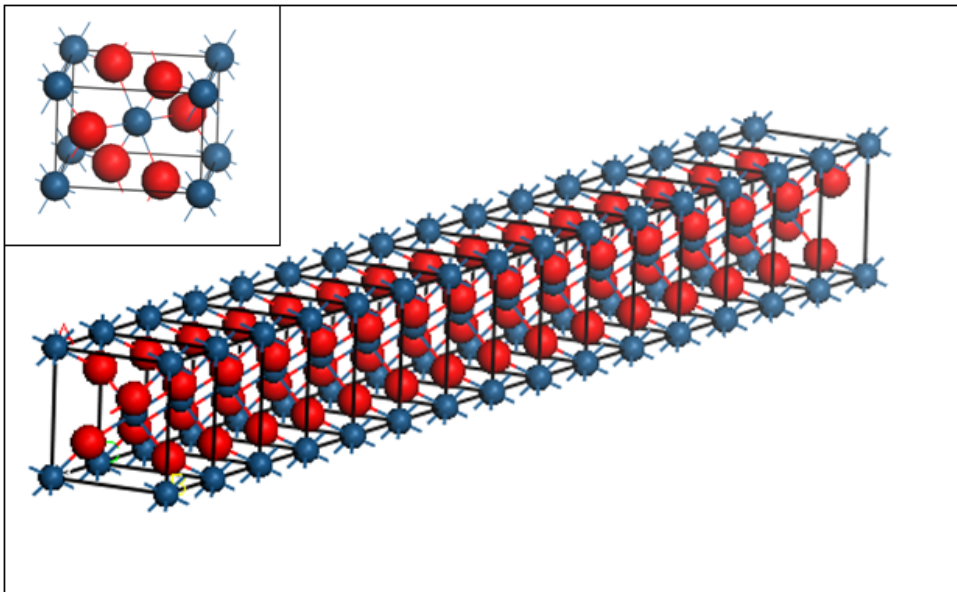
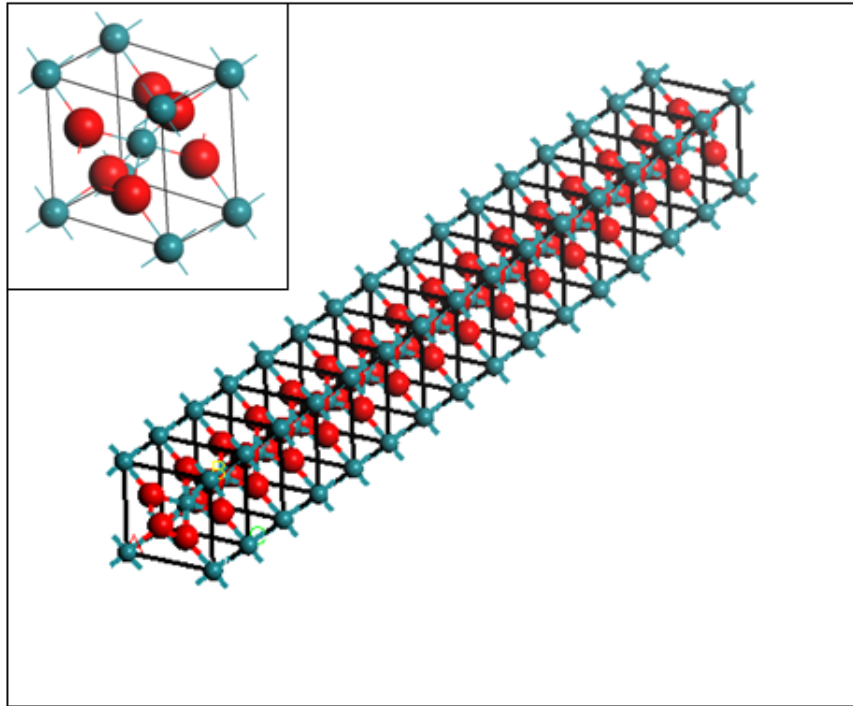


Fig. 3.2 The structure of 1x1 nanowire for RuO_2 (upper panel) and IrO_2 (lower panel). The picture of the top-left corner is its bulk structure.

The 2x2 nanowires have the same periodicity along the z direction as the bulk crystal. The periodicity of 2x2 nanowires is two repeated primitive cells and two empty primitive cells along the x and y direction. Thus, the lattice parameters become $a=b=18.24 \text{ \AA}$, $c=3.16 \text{ \AA}$ for the RuO_2 and $a=b=17.96 \text{ \AA}$, $c=3.15 \text{ \AA}$ for the IrO_2 . We show the structure of 2x2 nanowires in Fig. 3.3.

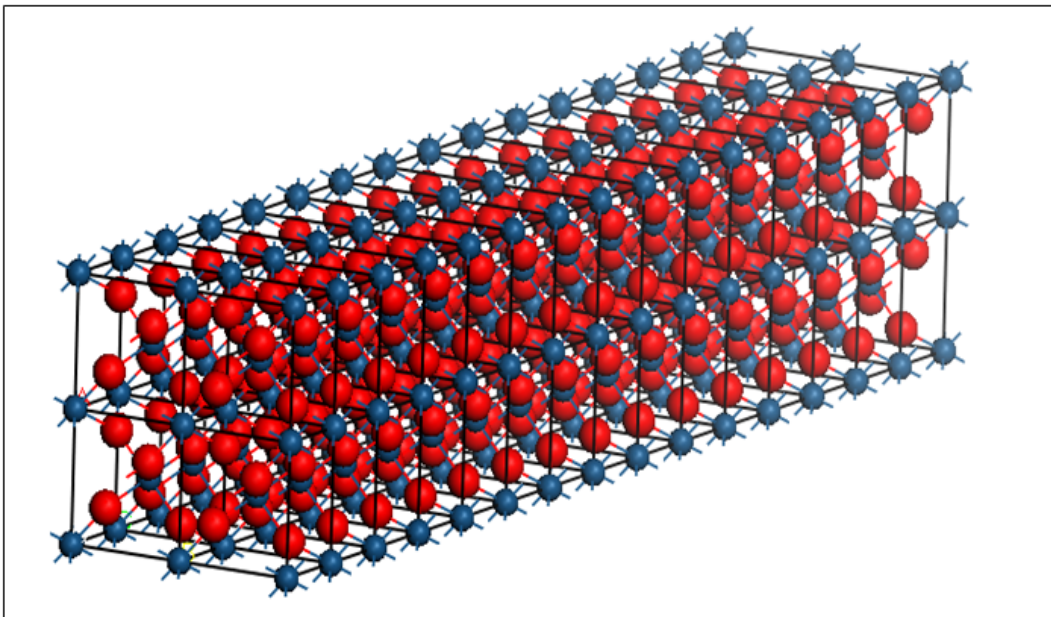
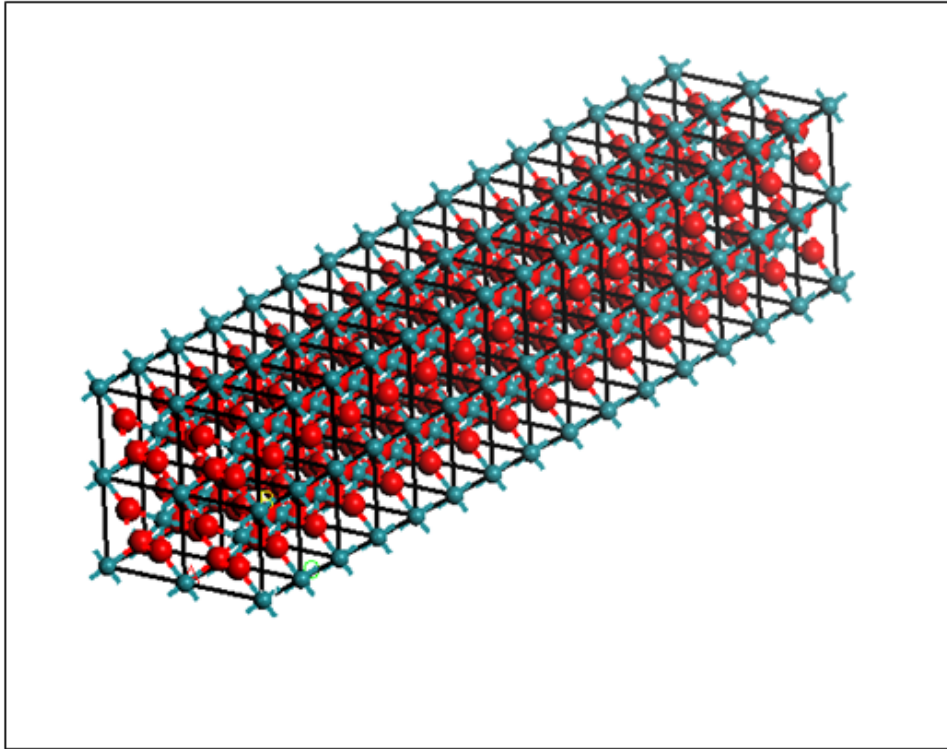


Fig. 3.3 The structure of 2x2 nanowire for RuO_2 (upper panel) and IrO_2 (lower panel).

The reason for the repetition of two empty primitive cells in the x and y direction nanowires is to avoid the interactions between wires. It must be greater than 9 \AA which is about the size of the two primitive cells.

3-2 VASP Calculation

In the previous section, we have introduced the structures of the RuO_2 and IrO_2 . We relax the structures of the RuO_2 and IrO_2 by applying the VASP code. VASP is an ab-initio package for performing quantum mechanical molecular dynamics simulations using the pseudopotential or the projector-augmented wave method and a plane wave basis set. The approach implemented in VASP is based on the local density approximation with the free energy variational quantity. Forces can be calculated with VASP and used to relax atoms into their ground state.

VASP have four input files, INCAR, KPOINTS, POSCAR, and POTCAR. The POSCAR file contains the lattice geometry and the atom positions. We apply the software “Material Studio” to construct the positions of atoms in the crystal material and nanowires. The results of the coordinates obtained from the “Material Studio” have entered into the POSCAR file in VASP. The example is shown in Fig.3.4.

```
IrO2
1.000
 4.4983000  0.0000000  0.0000000
 0.0000000  4.4983000  0.0000000
 0.0000000  0.0000000  3.1547000
2 4
Direct
 0.000000  0.000000  0.000000
 0.500000  0.500000  0.500000
 0.308200  0.308200  0.000000
-0.308200 -0.308200  0.000000
 0.191800  0.808200  0.500000
 0.808200  0.191800  0.500000
```

Fig. 3.4 The contents of the POSCAR file.

The first line is treated as a comment line. The data from the third to fifth lines are the lattice constants for a, b and c respectively. The data from the eighth to final lines are the positions of atoms in Cartesian coordinates.

The POTCAR file contains the pseudopotential for each atomic species used in the calculations. The file is large, so we only show the partial contents of the POTCAR file.

```

US Ru
8.0000000000000000
parameters from PSCTR are:
VRHFIN =Ru: s1 d7
LEXCH  = CA
EATOM  = 690.4189 eV, 50.7444 Ry
GGA    = -7.0512 -6.7388 1.2442 -6.1224 eV

TITEL  = US Ru
LULTRA = T use ultrasoft PP ?
IUNSCR = 1 unscreen: 0-lin 1-nonlin 2-no
RPACOR = 1.050 partial core radius
POMASS = 101.070; ZVAL = 8.000 mass and valenz
RCORE  = 2.650 outmost cutoff radius
RWIGS  = 2.650; RWIGS = 1.402 wigner-seitz radius (au A)
ENMAX  = 203.565; ENMIN = 152.674 eV
EAUG   = 340.989

RCLOC  = 1.830 cutoff for local pot
LCOR   = T correct aug charges
RMAX   = 3.232 core radius for proj-oper
QCUT   = -3.868; QGAM = 7.736 optimization parameters

```

Fig. 3.5 The partial contents of POTCAR file for local-density approximation.

The KPOINTS file contains the coordinates and weights of the k-point mesh. We choose the default settings to generate k-point, and we only need to specify the subdivisions in the first Brillouin zone in each direction. The content of the KPOINTS file is shown in Fig.3.6.

```

Automatic generation
0
Monkhorst-Pack
10 10 10
0 0 0
~
~

```

Fig. 3.6 The contents of the KPOINTS file.

The first line is treated as a comment line. In the second line, the number 0 is specified to generate the k-point automatically. The third line starting with “M” selects the Monkhorst-Pack scheme for k-points. The fourth line shows (10 10 10) which means to generate 10x10x10 k-point in the first Brillouin zone.

The INCAR file is the most important input file in VASP. It contains a lot of useful parameters. We only show in Fig.3.7 the parameters other than the default values in the INCAR file.

```

System = IrO2
ISTART = 0
MAGMOM= 1 1 0 0 0 0
PREC = Accurate
EDIFF = 1E-5
IBRION = 1
ISIF = 2
ISMEAR = 1
SIGMA = 0.2
NSW = 50
~
~

```

Fig. 3.7 The contents of the INCAR file.

On the first line it contains the job title which can be arbitrarily named. When we run a new job, ISTART must be set to 0. One can set the “PREC=High or Accurate” to increase the precision in the calculations at cost of more computer time. ISMEAR in the INCAR file determines how the partial occupancies f_{nk} are set for each wave function. We choose the ISMEAR equal to 1 according to the recommendation by the VASP manual, which recommends that the metals use ISMEAR=1 in the relaxation processes. The conductivities of RuO_2 and IrO_2 are close to the properties of metal. The tag NSW defines the number of ionic steps. We do not display other parameters which are set to the default values.

With the four input files in VASP, the jobs can be submitted to PC Clusters for calculations. The output files are shown in Fig.3.8.

```

[bou@spark bulk]$ ls
band  CONTCAR  IBZKPT  move  PCDAT  qscript.vasp.mpi-dell  vasprun.xml
CHG   DOSCAR   INCAR   OSZICAR  POSCAR  vasp.mpi.err           WAVECAR
CHGCR EIGENVAL KPOINTS OUTCAR  POTCAR  vasp.mpi.log           XDATCAR

```

Fig. 3.8 All output files of the VASP.

To calculate the force constants we need to move the positions of atoms, which are stored in the file CONTCAR containing the information of atom positions after relaxation. The OUTCAR file contains other useful information such as forces, potentials, free energy, etc.

3-3 Phonon dispersion relation

In this section we introduce the program “PHON” which is applied to calculate the

phonon dispersion relation of the crystal. The program “PHON” is able to calculate the phonon dispersion relations incorporated with any other program which is capable of calculating the force matrices of the system.

The program “PHON” has three input files, INPHON, FORCES and POSCAR. The POSCAR file of the program “PHON” needs the relaxed atom positions which are given by the CONTCAR file, one of the output files in the VASP program.

The INPHON file is the central input file of “PHON”. The parameters in the INPHON file are shown in Fig.3.9.

```
# symmetrize force constant matrix
#   LSYMM=.FALSE.
NTI = 20

# generate superlattice
LSUPER = .T.;
NDIM = 1 1 1

# number of ions types and massesq
NTYPES = 2; MASS = 192.217 16.000
USETHIS = .T. .F.

# free energy calculation
LFREE = .F.; TEMPERATURE = 0

# q points section
LRECIP = .T.
ND = 1; NPOINTS = 50
QI = 0 0 0
QF = 0 0 1

# density of states
LGAMMA = .FALSE.
QA = 12; QB = 12; QC = 12
DOSIN = 0; DOSEND = 25; DOSSTEP = 0.1; DOSSMEAR = 0.2

# write force constant matrix
LFORCEOUT = .T.

# verbosity
IPRINT = 0
~
```

Fig. 3.9 The contents of the INPHON file.

Most of the parameters are set to the default values. It should pay attention to the LSUPER tag which must be set to LSUPER=.T. in the INPHON file. In the trial run of “PHON” program, we only need two files POSCAR and INPHON where the tag LSUPER is set to “True”. The trial run will generate the DISP file, where the displacement vectors of the atoms are given. These displacement vectors tell us how to move the positions of atoms and are applied to calculate the force matrices by using the VASP

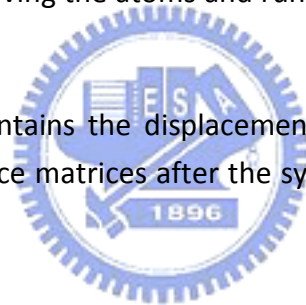
program. The example of the DISP file is shown in Fig.3.10.

```
" 1 0.00889225 0.00000000 0.00000000 "  
" 1 0.00000000 0.00000000 0.01267949 "  
" 3 0.00889225 0.00000000 0.00000000 "  
" 3 0.00000000 0.00000000 0.01267949 "  
~  
~
```

Fig. 3.10 The contents of the DISP file.

The first line contains the information of how the atoms must be displaced. The 1 and 3 in the first column represent the first atom and the third atom, respectively. The three numerals in the second to fourth columns represent the relative displacement vectors of atoms. When we have these data, we reconstruct the POSCAR in the VASP program using the relaxed coordinates of atoms from the CONTCAR file in the VASP program and displacement vectors in the DISP file from the PHON program. We fix the atoms positions after moving the atoms and run the VASP program again to obtain the force matrices.

The FORCES file contains the displacements and the force information of each atom. We obtain the force matrices after the system relaxed by VASP. The example is shown in Fig. 3.11.



```

4
1 0.00889225 0.00000000 0.00000000
   -0.001773 -0.003024 0.000000
   -0.002927 -0.005103 0.000000
    0.003858 -0.000375 0.000000
    0.003957 0.000299 0.000000
   -0.001682 0.004604 0.000000
   -0.001433 0.003599 0.000000
1 0.00000000 0.00000000 0.01267949
   0.000000 0.000000 0.001116
   0.000000 0.000000 0.002504
   0.000015 0.000015 -0.000186
   -0.000015 -0.000015 -0.000186
   0.000202 -0.000202 -0.001624
   -0.000202 0.000202 -0.001624
3 0.00889225 0.00000000 0.00000000
   -0.001014 0.001387 0.000000
   -0.000589 0.001031 0.000000
   -0.003813 0.004174 0.000000
    0.007279 -0.005570 0.000000
    0.003140 0.003554 0.000000
   -0.005003 -0.004575 0.000000
3 0.00000000 0.00000000 0.01267949
   -0.002829 -0.002829 0.000278
   -0.003893 -0.003893 -0.000653
    0.004419 0.004419 -0.000912
    0.001791 0.001791 -0.000879
    0.000438 0.000074 0.001083
    0.000074 0.000438 0.001083

```

Fig. 3.11 The contents of the FORCES file.

The number of the first line is specified the number of displacements. The second line contains the information of how the atoms must be displaced. The data from the third to eighth line are the forces on all the atoms in the supercell. According to the information of the DISP file, there are four force matrices in the FORCES file.

Before we run the PHON, the tag LSUPER in the INPHON file must be set "F". With the three input files, the jobs can be submitted to PC Clusters for calculations. The results are shown in Fig. 3.12.

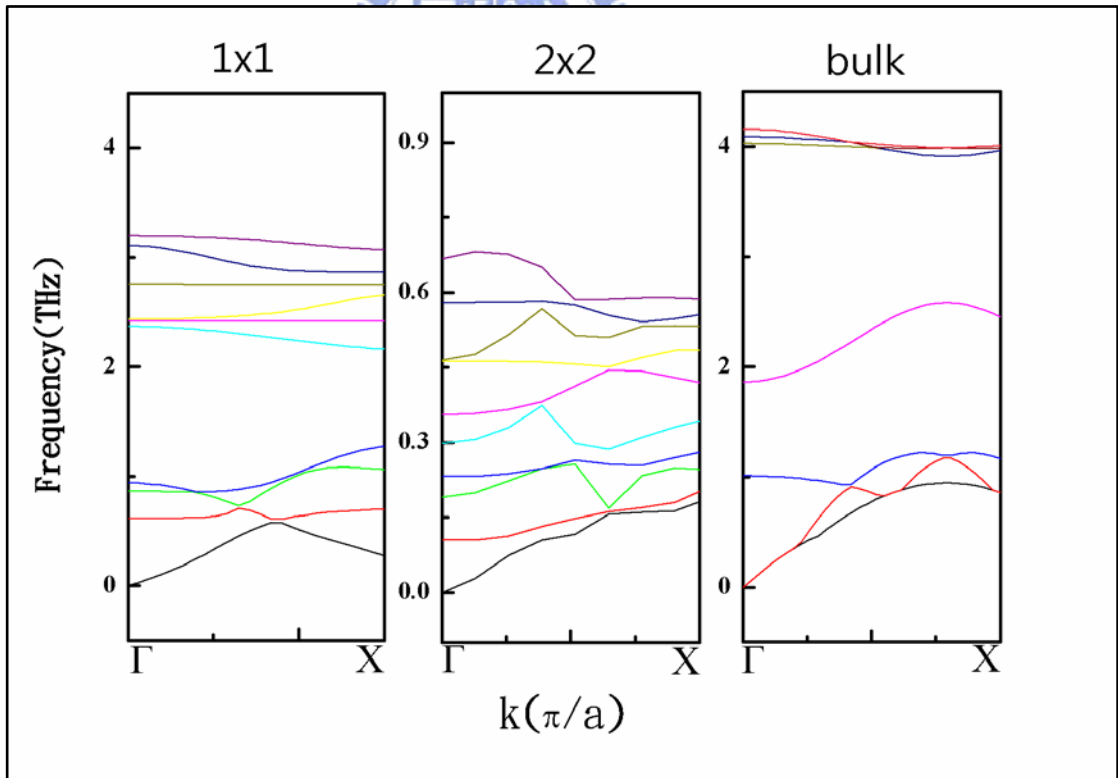
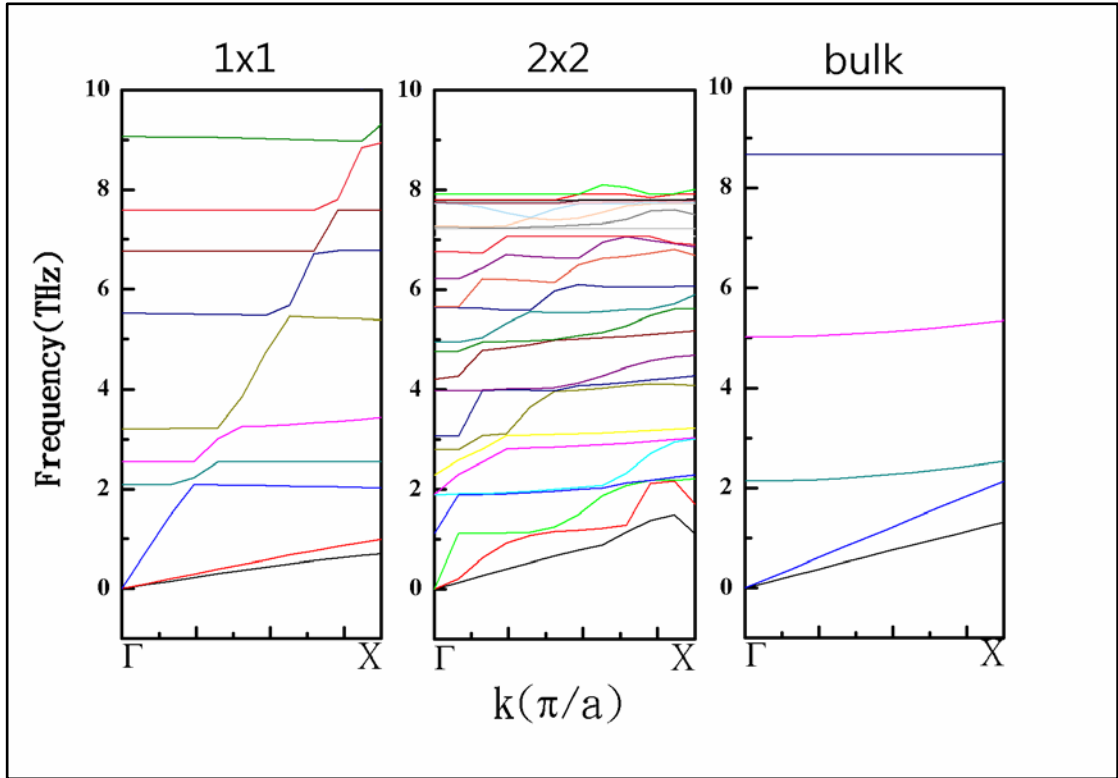


Fig. 3.12 Phonon dispersion relation for the RuO_2 (upper panel) and IrO_2 (lower panel).

For the bulk and 1x1 nanowires, there are three acoustic branches and fifteen

optical branches. There are twelve acoustic branches and sixty optical branches in the 2x2 nanowires. The value of sound velocity plays an important part in our study. The sound velocity is obtained from the phonon dispersion relation. The group velocity of the phonon is defined as $V_g = \frac{d\omega}{dk}$, so we are able to calculate the sound velocity from the phonon dispersion relation of the the acoustic phonon. These quantities will be used late to calculate the resistivity of the bulk materials and nanowires.

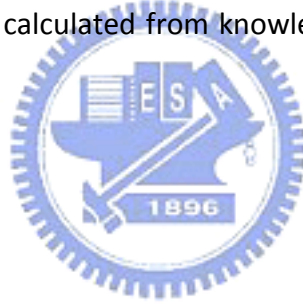
3-4 Matthiessen's rule²⁵

Theoretically, the resistivity is defined as

$$\rho = \frac{4\pi}{\Omega_p^2 \tau}, \quad (3.1)$$

where $\frac{1}{\tau}$ is the electron scatter rate and Ω_p is the plasma frequency. The plasma frequency tensor can be calculated from knowledge of the electronic structure and is given by

$$\Omega_p^2 = \frac{-8\pi e^2}{V} \sum_{nk} v_{nk}^2 \frac{\partial f_{nk}}{\partial \epsilon_{nk}}, \quad (3.2)$$



where V is the volume, the group velocity of phonon is $v_{nk} = \frac{1}{\hbar} \frac{\partial \epsilon_{nk}}{\partial k}$ and f_{nk} is the particle distribution function. The scattering rate for electron transport resulting from electron-phonon scattering is given by

$$\frac{\hbar}{\tau} = 4\pi k_B T \int_0^\infty \frac{d\omega}{\omega} \alpha^2 F(\omega) \left[\frac{\hbar\omega / 2k_B T}{\sinh(\hbar\omega / 2k_B T)} \right]^2, \quad (3.3)$$

where ω is the phonon frequency and $\alpha^2 F(\omega)$ is the spectral function.

Typically, the scattering rate for many metals follows a Bloch-Gruneisen type behavior. For acoustic mode phonons, $\alpha^2 F(\omega)$ will be replaced with its Debye approximation :

$$\alpha_{BG}^2 F(\omega) = 2\lambda_{BG} \left(\frac{\omega}{\omega_D} \right)^4 \theta(\omega_D - \omega), \quad (3.4)$$

where θ is the Heaviside step function, ω_D is the Debye frequency and λ_{BG} is the transport electron-phonon coupling constant in the Bloch-Gruneisen model²⁶. One can plug Eq. (3.4) into Eq.(3.3) and obtain the scattering rate

$$\begin{aligned}
\frac{\hbar}{\tau^{BG}} &= 8\pi k_B T \lambda_{BG} \int_0^{\infty} \frac{d\omega}{\omega} \left(\frac{\omega}{\omega_D}\right)^2 \theta(\omega_D - \omega) \left[\frac{\hbar\omega / 2k_B T}{\sinh(\hbar\omega / 2k_B T)}\right]^2 \\
&= 8\pi k_B T \lambda_{BG} \int_0^{\frac{\Theta_D}{T}} \frac{dx}{x} \left(\frac{T}{\Theta_D} x\right)^4 \left[\frac{x^2}{4 \sinh^2\left(\frac{x}{2}\right)}\right] \\
&= 8\pi k_B T \lambda_{BG} \int_0^{\frac{\Theta_D}{T}} \left(\frac{T}{\Theta_D}\right)^4 \frac{x^5}{4 \sinh^2\left(\frac{x}{2}\right)} dx,
\end{aligned} \tag{3.5}$$

where $x \equiv \frac{\hbar\omega}{k_B T}$, $\frac{d\omega}{\omega} = \frac{dx}{x}$

and $\Theta_D = \frac{\hbar\omega_D}{k_B}$, $\frac{\omega}{\omega_D} = \frac{k_B T}{\hbar} x \cdot \frac{\hbar}{k_B \Theta_D} = \frac{T}{\Theta_D} x$.

Here, Θ_D is the Debye temperature corresponding to the maximum phonon energy in the Debye approximation. Substituting Eq.(3.5) and Eq.(3.2) into Eq.(3.1), the resistivity can be written as

$$\rho_{BG}(T) = \frac{32\pi^2}{\hbar\Omega_p^2} k_B T \lambda_{BG} \left(\frac{T}{\Theta_D}\right)^4 \int_0^{\frac{\Theta_D}{T}} \frac{x^5}{4 \sinh^2\left(\frac{x}{2}\right)} dx. \tag{3.6}$$

If the temperature is smaller than Debye temperature, the result of the integral equation approaches to a constant, and thus the resistivity in the Bloch-Gruneisen model is proportional to T^5 . The above equation is applied to calculate the resistivity of the RuO_2 and IrO_2 nanowires.

An additional contribution due to the coupling between electrons and optical mode phonons can be considered as well. The electron-phonon contribution can be obtained by substituting $\alpha_E^2 F(\omega)$ in the Einstein approximation.

$$\alpha_E^2 F(\omega) = \frac{1}{2} \omega_E \lambda_E \delta(\omega - \omega_E). \tag{3.7}$$

Substituting Eq.(3.7) into Eq.(3.3) , the equation is shown as

$$\begin{aligned}
\frac{\hbar}{\tau^E} &= 2\pi k_B T \lambda_E \int_0^\infty d\omega \frac{\omega_E}{\omega} \delta(\omega - \omega_E) \left[\frac{\hbar\omega / 2k_B T}{\sinh(\hbar\omega / 2k_B T)} \right]^2 \\
&= 2\pi k_B T \lambda_E \left[\frac{\hbar\omega_E / 2k_B T}{\sinh(\hbar\omega_E / 2k_B T)} \right]^2 \\
&= 2\pi k_B T \lambda_E \left[\frac{\Theta_E / 2T}{\sinh(\Theta_E / 2T)} \right]^2,
\end{aligned} \tag{3.8}$$

where $\Theta_E = \frac{\hbar\omega_E}{k_B}$.

From Eq.(3.8) and Eq.(3.2) the resistivity is given by

$$\rho_E(T) = \frac{8\pi^2}{\hbar\Omega_p} k_B T \lambda_E \left[\frac{\Theta_E / 2T}{\sinh(\Theta_E / 2T)} \right]^2. \tag{3.9}$$

The optical mode coupling term is treated using Einstein approximation with a single phonon frequency corresponding to the energy $k_B\Theta_E$.

Besides the electron-phonon scattering, there is another term to influence the resistivity which is electron-electron scattering. The resistivity depends on T^2 and can be written as

$$\rho_{ee}(T) = A_{ee} T^2. \tag{3.10}$$

According to the Matthiessen's rule these three contributions [Eq.(3.6), Eq.(3.9), Eq.(3.10)] are additive and independent of each other. The total resistivity $\rho(T)$ is the sum of the residual resistivity ρ_0 , Eq.(3.6), Eq.(3.9) and Eq.(3.10), it can be expressed as follow.

$$\rho(T) = \rho_0 + \rho_{BG}(T) + \rho_E(T) + \rho_{ee}(T). \tag{3.11}$$

At low temperature, the resistivity is dominated by impurities, vacancies, and various other defects. For low defect concentrations, these contributions are frequently assumed to be independent of the temperature; the T=0 limit being defined as the residual resistivity ρ_0 . The resistivity due to the electron-electron scattering can be neglected at low temperature because in practice in transition metal the

parameter A_{ee} is only of the order of $10^{-5} (\mu\Omega \cdot cm / K^2)$.

3-5 Results and Discussion

3-5-1 Debye temperature calculation^{27,28}

The Debye temperature is defined as

$$\Theta_D = \frac{\hbar v}{k_B} \left(\frac{6\pi^2 N}{V} \right)^{\frac{1}{3}}, \quad (3.12)$$

where v is the velocity of sound, N is the number of primitive cells in the sample and V is the volume of the sample. From the phonon dispersion relation together with the parameters known from the structures of nanowires, we can calculate the sound velocity v and the Debye temperature from our theoretical calculations.

The temperature dependence of the resistivity at $T < \Theta_D$ is determined by the electron-phonon contribution only. When the ratio of $\frac{\Theta_D}{T}$ is large, the resistivity is proportional to T^5 . Oppositely, the ratio of $\frac{\Theta_D}{T}$ is small, the resistivity gives a T dependence. Our research is focus on the resistivity varies as T^5 in Bloch-Grüneisen equation. Thus, the low temperature system is mainly investigated for us. The results are shown in Fig.3.13 and we can see that the Debye temperature increases as the sizes of the system increase.

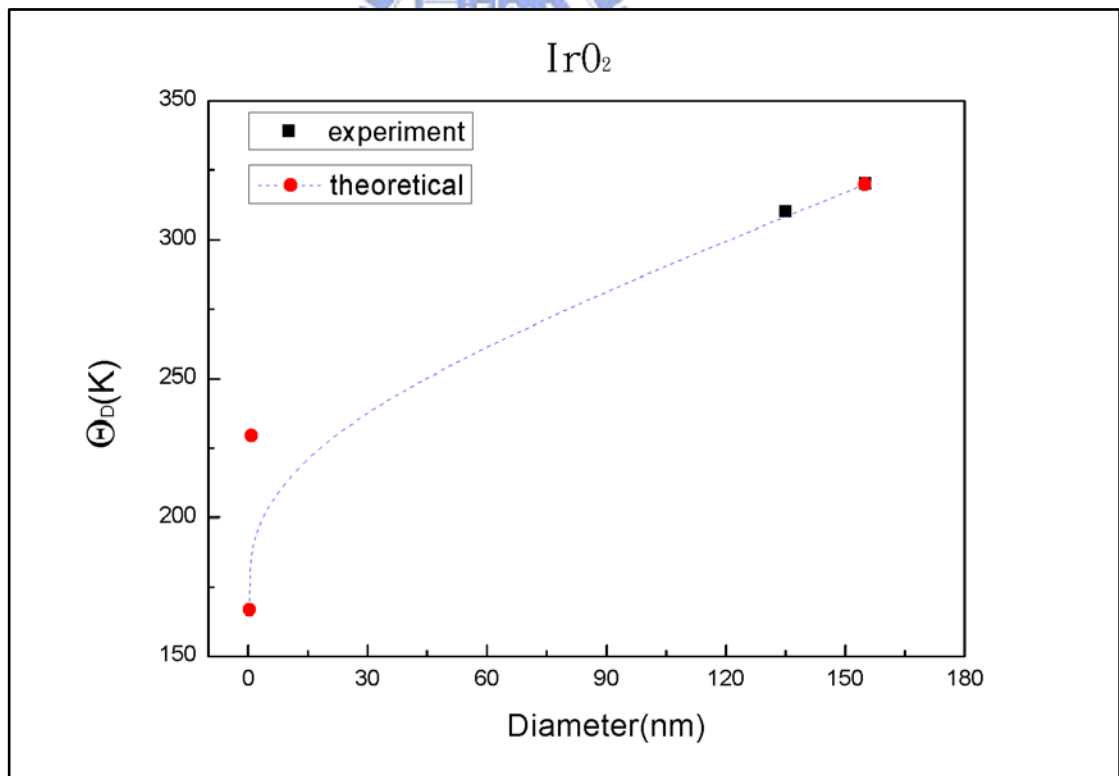
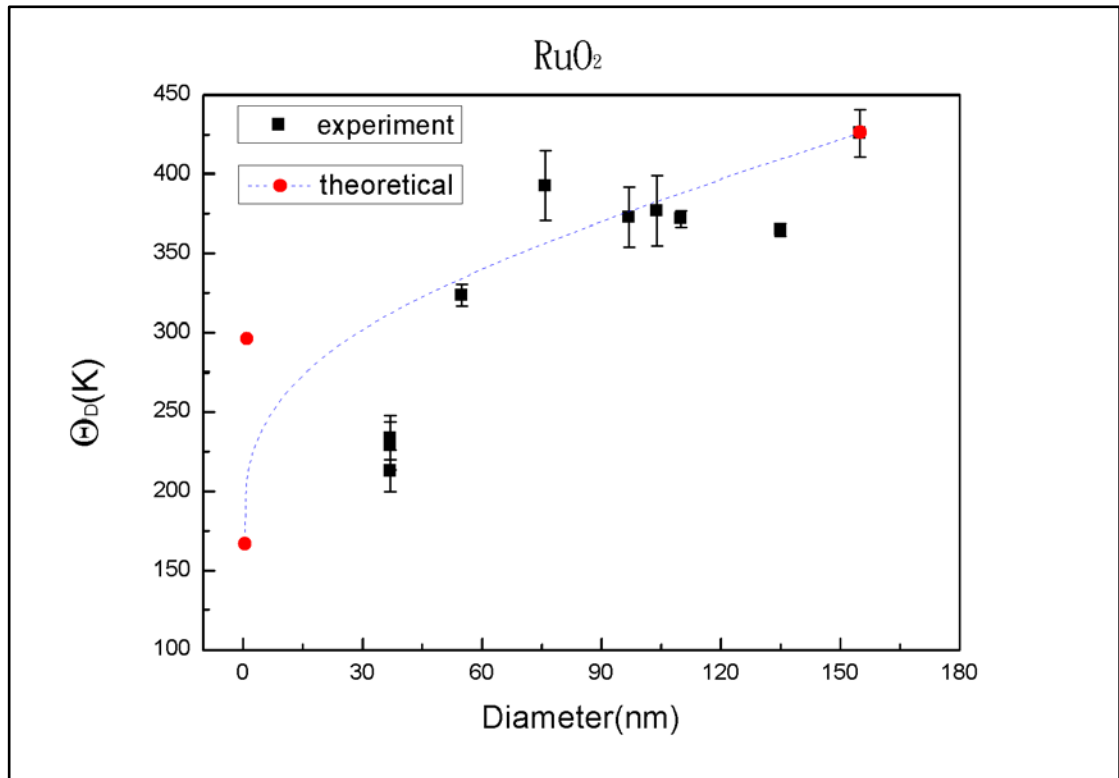
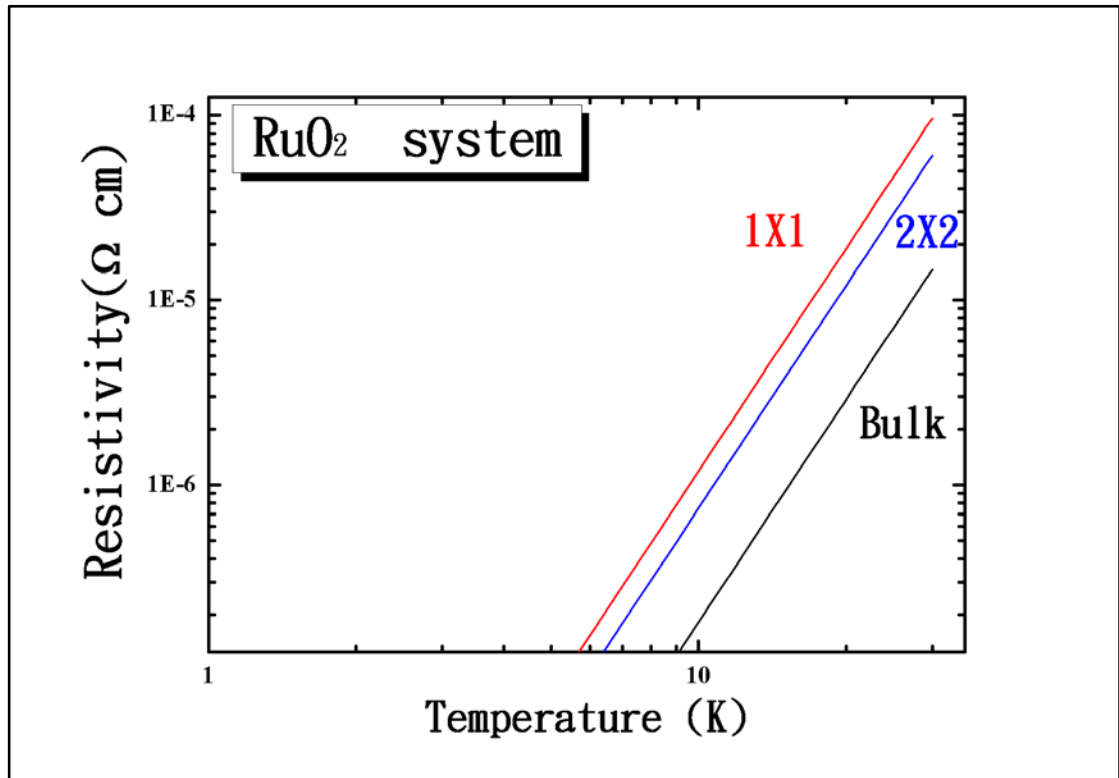


Fig. 3.13 The dependence of the Debye temperature in RuO_2 (upper panel) and IrO_2 (lower panel) on the diameters of the nanowires.

3-5-2 Bloch-Gruneisen Model calculation

We investigate the resistivity of the nanowires due to the electron-phonon scattering. It gives a T^5 dependence at low temperature. The results of the resistivity versus the temperature in RuO_2 and IrO_2 are shown in Fig.3.14.



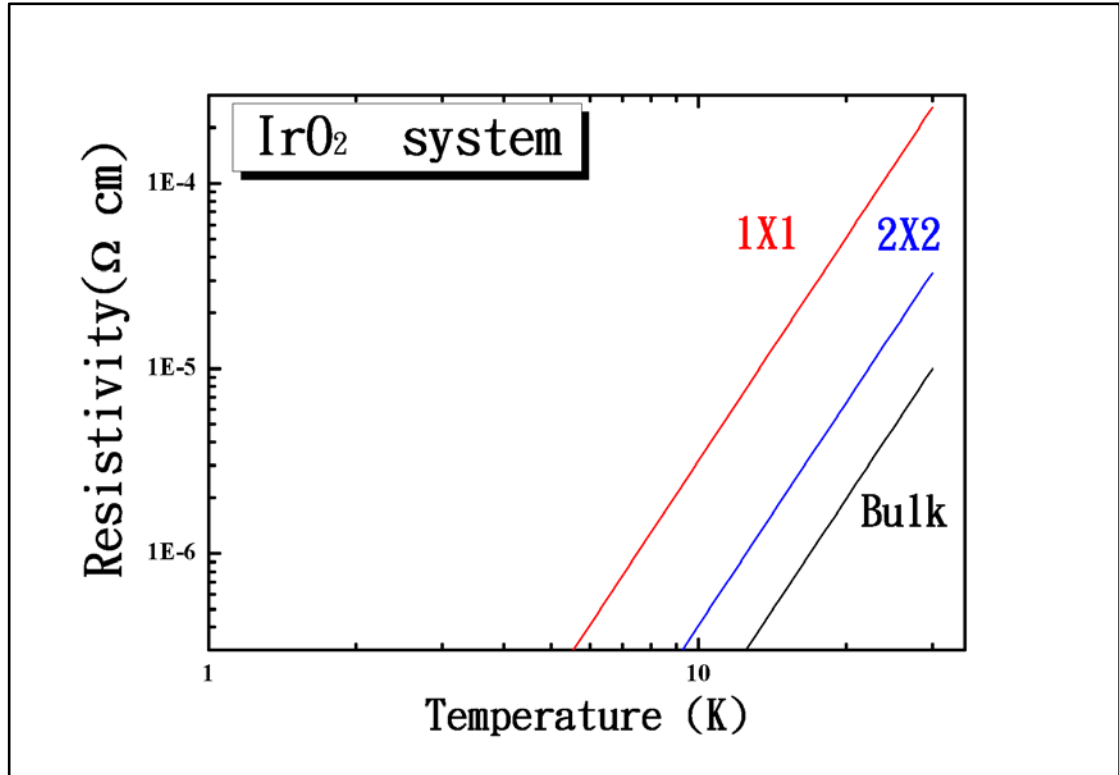


Fig. 3.14 The resistivity of RuO_2 (upper panel) and IrO_2 (lower panel) nanowires due to the interactions between electrons and the acoustic phonons.

From the frequency dispersions, we observe that the velocity of phonon in the 1x1 nanowire is the slowest. The sound velocities increase as the diameters of the wires increase. From the approximately expression $\omega = \sqrt{\frac{k}{m}}$ for a harmonic oscillator from the Hooke's law, we realize that the sound velocity decreases as the force constants decrease. We conjecture that the nanowires with smaller diameters have smaller binding force and smaller sound velocity, and thus are less stable.

At low temperatures, we observe that the resistivity increases as the temperature rises. The lattice vibrations are more violent as the temperatures rise, which generate more phonons. Consequently, the probability of electron-phonon collision increases and it causes the conductivity to decrease. The resistivity varies with T^5 according to the Bloch-Gruneisen equation. At a given temperature, the resistivity decreases as the diameter of the nanowire. The decrease of the sound velocity is due to the decrease of the effective strength of the force which binds the nanowire.

Chapter4 Conclusion

We have investigated the Debye temperature and the conductivity for RuO_2 and IrO_2 nanowires due to the electron-phonon interactions described by the Bloch-Gruneisen theorem.

Firstly, we employ the projected augmented wave method as implemented in Vienna Ab initio Simulation Package (VASP) to investigate systems of RuO_2 and IrO_2 bulk crystal using density-functional theory calculations with exchange correlation energy in the local density approximation. All atoms are relaxed until the forces are smaller than 0.001 eV/\AA . The optimized the RuO_2 bulk crystal has lattice parameters: $a=b=4.56 \text{ \AA}$, $c=3.16 \text{ \AA}$, which are in good agreement with the experimental values, $a=b=4.500\pm 0.005 \text{ \AA}$, $c=3.101\pm 0.006 \text{ \AA}$. In the same way we relax the geometry for the IrO_2 bulk crystal, and obtain the lattice parameters: $a=b=4.49 \text{ \AA}$, $c=3.15 \text{ \AA}$, which are also in good agreement with the experimental values.

Secondly, we build up the super cell structures of nanowires along (001) direction based on the geometry of the relaxed bulk systems as the initial input. We have built up two different diameters of RuO_2 and IrO_2 nanowires: (1) one unit cell (1x1) and (2) four unit cells (2x2) in the directions parallel to the direction of charge current. Nanowires are infinite along the (001) direction and are also separated by a vacuum region in the x and y directions. We also relax the geometry of nanowires following the same method using VASP as described in the above, where have used (1x1x10) k-point Monkhorst-Pack meshes in our calculations.

The VASP is applied to calculate the force matrix and the PHON is applied to calculate the phonon dispersion relations of the bulk and nanowires. For the IrO_2 system, the Fermi energies of the bulk crystal, 1x1 wire, and 2x2 wire are 6.19 eV, 5.84 eV, and 3.39 eV, respectively. Since the diameters of the nanowires (4.49 Å for bulk crystal and 13.47 Å and 17.96 Å for 1x1 and 2x2 wires, respectively) are comparable with the Fermi wave lengths, the systems may display strong quantum mechanical effects. We observe that the sound velocities and the Debye temperatures are strongly suppressed when the decreasing diameters of the nanowires are comparable to the Fermi wave lengths.

Using the phonon dispersion obtained from the PHON and VASP, we calculate the conductivities of nanowires due to the interactions between electrons and the vibrations of lattice. The resistivity varies as T^5 at low temperatures according to the Bloch-Gruneisen equation. At a given temperature, we observe that the conductivity due to electron-phonon interactions decreases as the diameters of nanowires decrease. The reason for the decrease of resistivity with the diameters of nanowires is

that the sound velocities also decrease due to the decrease of the force constants as the diameters of nanowires decrease. Since the size effects observed in our calculations are much enhanced when the diameters of the nanowires are comparable with the Fermi wave length, we conjecture that the size effects stem from the quantum mechanical effects.



Chapter5 Reference

- 1 J. H. Xu, T. Jarlborg, and A. J. Freeman, Phys. Rev. B **40**, 7939 (1989).
- 2 K. M. Glassford and J. R. Chelikowsky, Phys. Rev. B **47**, 1732 (1993).
- 3 B. C. Passenheim and D. C. McCollum, J Chem Phys **51**, 320 (1969).
- 4 W. D. Ryden, A. W. Lawson, and C. C. Sartain, Phys. Rev. B **1**, 1494 (1970).
- 5 J. J. Lin, S. M. Huang, Y. H. Lin, T. C. Lee, H. Liu, X. X. Zhang, R. S. Chen, and Y. S. Huang, J. Phys.-Condes. Matter **16**, 8035 (2004).
- 6 Y. H. Lin, Y. C. Sun, W. B. Jian, H. M. Chang, Y. S. Huang, and J. J. Lin, Nanotechnology **19**, 8 (2008).
- 7 Y. L. Liu, Z. Y. Wu, K. J. Lin, J. J. Huang, F. R. Chen, J. J. Kai, Y. H. Lin, W. B. Jian, and J. J. Lin, Appl. Phys. Lett. **90**, 3 (2007).
- 8 M. Marsman and J. Furthmuller, *Vienna Ab-initio Simulation Package* (2009).
- 9 D. Alfe, *PHON* (2005).
- 10 B. C. Taylor, *Introduction to Solid-State Theory*.
- 11 P. Hohenberg and W. Kohn, Phys. Rev. **136**, B864 (1964).
- 12 W. Kohn and L. J. Sham, Phys. Rev. **140**, A1133 (1965).
- 13 C. Espejo and R. R. Rey-Gonzalez, Revista Colombiana De Fisica **39**, 407 (2006).
- 14 D. R. Hamann, M. Schluter, and C. Chiang, Phys. Rev. Lett. **43**, 1494 (1979).
- 15 I. Morrison, D. M. Bylander, and L. Kleinman, Phys. Rev. B **47**, 6728 (1993).
- 16 L. Kleinman and D. M. Bylander, Phys. Rev. Lett. **48**, 1425 (1982).
- 17 D. Vanderbilt, Phys. Rev. B **41**, 7892 (1990).
- 18 M. Y. Chou, Phys. Rev. B **45**, 11465 (1992).
- 19 M. Corradini and R. Del Sole, Phys. Rev. B **66**, 193101 (2002).
- 20 D. Ceperley and B. Alder, Science **231**, 555 (1986).
- 21 C. Kittel, *Introduction to Solid State Physics*.
- 22 D. Alf, G. D. Price, and M. J. Gillan, Phys. Rev. B **64**, 045123 (2001).
- 23 G. Kresse, J. Furthmuller, and J. Hafner, Europhys. Lett. **32**, 729 (1995).
- 24 D. A. Huckaby and Z. W. Salsburg, Journal of Chemical Physics **53**, 2304 (1970).
- 25 K. M. Glassford and J. R. Chelikowsky, Phys. Rev. B **49**, 7107 (1994).
- 26 M. P. Marder, *Condensed Matter Physics*.
- 27 M. V. Kamalakar and A. K. Raychaudhuri, Phys. Rev. B **79**, 8 (2009).
- 28 M. J. Huang, T. M. Chang, C. K. Liu, and C. K. Yu, Int. J. Heat Mass Transf. **51**, 4470 (2008).